Downloaded from www.rnajournal.org on February 14, 2006

The brome mosaic virus RNA3 intergenic replication enhancer folds to mimic a tRNA TpsiC-stem loop and is modified in vivo

T. Baumstark and P. Ahlquist

RNA 2001 7: 1652-1670

References

Article cited in:
http://www.rnajournal.org/cgi/content/abstract/7/11/1652#otherarticles

Email alerting service

Receive free email alerts when new articles cite this article - sign up in the box at the top right corner of the article or **click here**

Notes

To subscribe to *RNA* go to:
http://www.rnajournal.org/subscriptions/

© 2001 RNA Society

Downloaded from www.rnajournal.org on February 14, 2006

RNA (2001), *7*:1652–1670. Cambridge University Press. Printed in the USA.
Copyright © 2001 RNA Society.
DOI: 10.1017.S1355838201018076

The brome mosaic virus RNA3 intergenic replication enhancer folds to mimic a tRNA TΨC-stem loop and is modified in vivo

TILMAN BAUMSTARK and PAUL AHLQUIST

Institute for Molecular Virology and Howard Hughes Medical Institute, University of Wisconsin-Madison, Madison, Wisconsin 53706, USA

ABSTRACT

The genome of brome mosaic virus (BMV), a positive-strand RNA virus in the alphavirus-like superfamily, consists of three capped, messenger-sense RNAs. RNA1 and RNA2 encode viral replication proteins 1a and 2a, respectively. RNA3 encodes the 3a movement protein and the coat protein, which are essential for systemic infection in plants but dispensable for RNA3 replication in plants and yeast. A subset of the 250-base intergenic region (IGR), the replication enhancer (RE), contains all *cis*-acting signals necessary for a crucial, early template selection step, the 1a-dependent recruitment of RNA3 into replication. One of these signals is a motif matching the conserved box B sequence of RNA polymerase III transcripts. Using chemical modification with CMCT, kethoxal, DMS, DEPC, and lead, we probed the structure of the IGR in short, defined transcripts and in full-length RNA3 in vitro, in yeast extracts, and in whole yeast cells. Our results reveal a stable, unbranched secondary structure that is not dependent on the surrounding ORF sequences or on host factors within the cell. Functional 5′ and 3′ deletions that defined the minimal RE in earlier deletion studies map to the end of a common helical segment. The box B motif is presented as a hairpin loop of 7 nt closed by G:C base pairs in perfect analogy to the TΨC-stem loop in tRNA^{Asp}. An adjacent U-rich internal loop, a short helix, and another pyrimidine-rich loop were significantly protected from base modifications. This same arrangement is conserved between BMV and cucumoviruses CMV, TAV, and PSV. In the BMV box B loop sequence, uridines corresponding to tRNA positions T_{54} and Ψ_{55} were found to be modified in yeast and plants to $5^{m}U$ and pseudouridine. Together with the aminoacylated viral 3′-end, this is thus the second RNA replication signal within BMV where the virus has evolved a tRNA structural mimicry to a degree that renders it a substrate for classical tRNA modification reactions in vivo.

Keywords: BMV; chemical probing; non-Watson–Crick base pairing; pseudouridine; ribothymidine; RNA structure; viral RNA replication

INTRODUCTION

Brome mosaic virus (BMV) belongs to the large alphavirus-like superfamily of plant and animal positive strand RNA viruses (Ahlquist, 1992). Its genome is divided among three capped, message-sense RNAs designated RNA1, RNA2, and RNA3. RNA1 and RNA2 encode RNA replication proteins 1a and 2a (French et al., 1986; Janda & Ahlquist, 1998) that contain three domains conserved with other members of the alphavirus superfamily. 1a (109 kDa) contains an N-terminal domain with m^7G methyltransferase and covalent GTP binding activities involved in viral RNA capping (Ahola & Ahlquist, 1999; Kong et al., 1999) and a C-terminal domain with similarity to DEAD box RNA helicases (Gorbalenya & Koonin, 1993). 2a (94 kDa) has a central domain with similarities to RNA-dependent RNA polymerases (Haseloff et al., 1984). RNA3 encodes the 3a protein, which is required for cell-to-cell movement in plants, and the coat protein, which is translated from a subgenomic mRNA (RNA4) and is required for encapsidation and long-range movement in plants (Allison et al., 1990).

Expressing 1a and 2a in *Saccharomyces cerevisiae* allows this yeast to support RNA replication and subgenomic RNA synthesis by RNA3 derivatives (Janda & Ahlquist, 1993) transcribed in vivo from suitable DNA cassettes (Ishikawa et al., 1997). In all aspects tested

Reprint requests to: Paul Ahlquist, Institute for Molecular Virology and Howard Hughes Medical Institute, University of Wisconsin-Madison, 1525 Linden Drive, Madison, Wisconsin 53706, USA; e-mail: ahlquist@facstaff.wisc.edu.

Downloaded from www.rnajournal.org on February 14, 2006

to date, BMV replication in yeast parallels that in plants, including dependence on 1a and 2a (Janda & Ahlquist, 1993; Ishikawa et al., 1997), association of replication complex with the endoplasmic reticulum (ER) membrane (Restrepo-Hartwig & Ahlquist, 1996, 1999; Chen & Ahlquist, 2000), and template specificity of RdRp extracts isolated from BMV infected plant (Miller & Hall, 1983) and yeast (Quadt et al., 1993, 1995).

In vitro and in vivo studies have identified 5′-, 3′- and intergenic sequences within RNAs 1, 2, and 3 that are required for efficient RNA replication and subgenomic RNA synthesis (reviewed in Sullivan & Ahlquist, 1997). The 3′ end of BMV RNAs and the RNAs of many other plant viruses mimic tRNA structurally (Ahlquist et al., 1981; Rietveld et al., 1983; Felden et al., 1994) and functionally in being charged with a specific amino acid (Loesch-Fries & Hall, 1982; Joshi et al., 1983). These ends further interact with tRNA nucleotidyl transferase (Joshi et al., 1983) and elongation factor EF-1a (Bastin & Hall, 1976). This conserved tRNA-like 3′ end functions as a negative-strand promoter in vitro (Dreher et al., 1984; Chapman & Kao, 1999), whereas correct positive strand initiation requires 5′-terminal sequences in vivo (Sullivan & Ahlquist, 1997) and a nontemplate guanylate added to the 3′-end of the minus strand in vitro (Sivakumaran & Kao, 1999). Apart from harboring the promoter for subgenomic RNA synthesis in the minus strand, the 250-base intergenic region (IGR) of RNA3 contains sequences in the plus sense that stimulate negative-strand synthesis from the 3′ end in vivo by approximately 100-fold (Quadt et al., 1995). A 150–200-base subset of the IGR, designated the intergenic replication enhancer (RE), stimulates RNA3 replication 50- to 100-fold in plant and yeast cells (French & Ahlquist, 1987; Sullivan & Ahlquist, 1999). A striking feature of this segment is a motif conserved with the box B consensus of RNA polymerase III promoters, which is subsequently transcribed into the TΨC stem-loop of tRNAs (French & Ahlquist, 1987). The same box B motif is found in the 5′ UTRs of RNA1 and RNA2 (Fig. 1). Deletion of the intergenic box B element in RNA3 or the 5′ box B in RNA2 seriously impairs replication of these RNAs in plant cells (Pogue et al., 1992; Smirnyagina et al., 1994) and in yeast (Sullivan & Ahlquist, 1999; Chen et al., 2001). A more varied, box B-related sequence is also found in the RNA3 5′ UTR (Fig. 1), but deleting this element does not inhibit RNA3 replication (Pogue et al., 1992).

In the absence of 2a protein and hence replication, 1a protein dramatically increases stability and accumulation of RNA3 in vivo without increasing its translation (Janda & Ahlquist, 1998). Genetic exchanges show that 1a and the RE are major determinants of template specificity in RNA3 replication (Traynor & Ahlquist, 1990; Pacha & Ahlquist, 1991). Partial deletions in the IGR stimulate or inhibit 1a-mediated RNA3 stabilization and RNA3 replication in parallel (Sullivan & Ahlquist, 1999), implying that 1a-mediated stabilization represents an early step of template recruitment from translation into the replication complex.

IGR segments containing the RE confer responsiveness to 1a mediated stabilization to nonviral RNAs (Sullivan & Ahlquist, 1999), showing that the RE is a self-contained functional unit. Deletion studies show that the minimal RE is 150 to 190 nt long and that box B is necessary but not sufficient to mediate 1a responsiveness. In the work presented here, we therefore investigated the secondary structure of the IGR to answer the following questions: Does the RE functional unit correspond to a structural unit? Within this, how is the box B sequence presented? Can we identify other subsegments within the RE that could be potential *cis*-acting elements? Is there evidence for tertiary structure formation or protein binding to specific sequences? Using chemical mapping in vitro and in vivo, computer predictions, and phylogenetic comparison, we found the IGR to fold into an unbranched structure bearing box B as a hairpin loop at the tip. Local conformational changes were observed under the influence of higher salt concentrations and magnesium, but no indication for stable tertiary interactions. Several regions of unusual structure, deviating from a standard A-type helix or single-stranded loop, could be identified. One of these, the box B hairpin loop, mimicked the TΨC-stem loop of canonical tRNA sufficiently that host enzymes modified the corresponding positions on BMV RNA3 to T and Ψ in vivo.

RESULTS

The intergenic region adopts a single conformation in vitro

As a foundation for structure mapping, we investigated whether the intergenic region has the potential to fold into one or more coexisting structures. In case of competing conformations, simple primer extension after chemical modification would yield an overlay of signals that would be difficult to analyze. To address this, three different in vitro transcripts were tested. Transcript IGR covered the intergenic region from the first 5′ nucleotide to immediately 3′ of the oligo-A tract (Fig. 1, bottom). Transcript $IGR^{\Delta 14}$ spanned the same sequence with the 14 nt containing box B (nt 1100–1113) deleted. IGRcp, a transcript used for chemical mapping, contained the entire intergenic region including the subgenomic promoter plus some flanking sequences from the coat protein ORF (Fig. 1, middle). This allowed us to use primer OL5 in mapping experiments covering the oligo-A tract and sequences further downstream.

These gel-purified transcripts were analyzed by native polyacrylamide gel electrophoresis after pretreatments previously shown to promote formation of alternate RNA structures (Steger et al., 1992; Baumstark & Riesner,

Downloaded from www.rnajournal.org on February 14, 2006

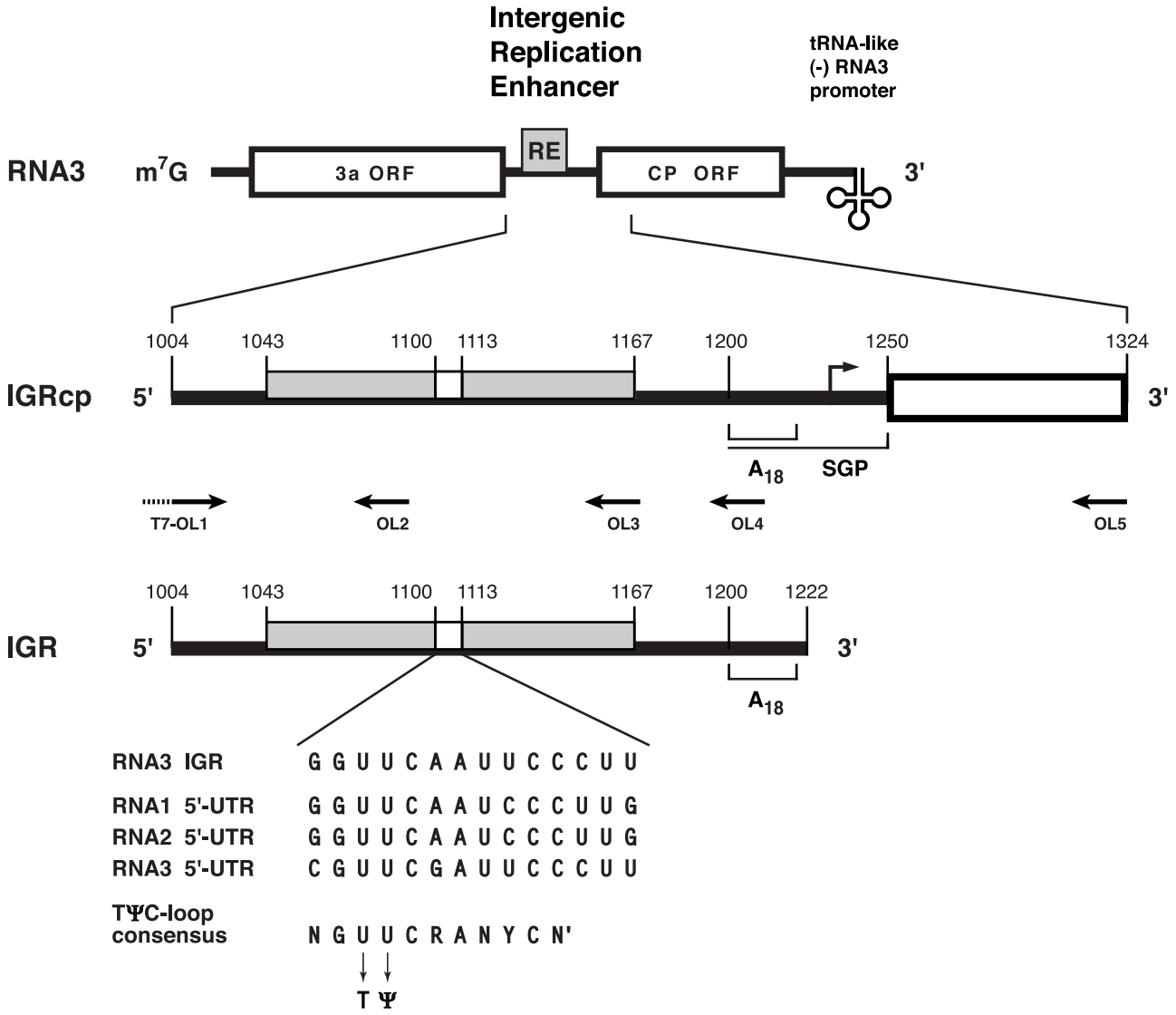

FIGURE 1. BMV RNA3 and constructs used in this study. Open reading frames for 3a protein and coat protein are shown as open boxes. *Cis*-acting signals involved in viral replication of 2,117-nt RNA3 (top, with methylated cap m^7G) include the tRNA-like 3′ end and the intergenic replication enhancer (RE, grey box), which contains the conserved box B element shown in sequence detail at the bottom along with the TΨC-loop consensus of tRNA; modifications found in natural tRNA are indicated below. Primer binding sites (OL1–5, arrows) and the promoter for subgenomic mRNA synthesis (SGP, RNA4 start site as bracketed arrow) including the oligo-A tract are shown with transcript IGRcp (middle).

1996). One set of samples was denatured at 95 °C in TE buffer and rapidly renatured on ice (Fig. 2, lanes LS^{snap}), which favors extended conformations with maximum separation of the backbone's charged phosphates, but can also trap kinetically favored structures that may be energetically far less stable than the equilibrium structures. Another set was denatured in higher ionic strength buffer (see Materials and Methods) and slowly renatured (Fig. 2, lanes HS^{slow}), which allows the structures to reach equilibrium, resulting in formation of the structure of lowest free energy and potentially a number of suboptimal structures. A third set was not treated further beyond gel purification (Fig. 2, lanes −).

For each transcript, electrophoresis under native conditions, that is, 18–20 °C in 0.2×TBE without magnesium (Fig. 2A) or 0.5xTBE with 5 mM Mg^{2+} (Fig. 2B), revealed a single, equivalently migrating band after snap-cooling in low salt (lanes 2, 5, and 8), slow renaturation in high salt (lanes 3, 6, and 9), or no pretreatment (lanes 1, 4, and 7). This implies that the IGR predominantly forms a single structure or closely related structures with indistinguishable electrophoretic mobility. Adding the 5′ portion of the coat protein open reading frame to the IGR transcript (Fig. 2B, lanes 4–6) did not change this behavior in IGRcp (Fig. 2B, lanes 1–3), nor did deletion of the box B region in $IGR^{\Delta 14}$ (Fig. 2B, lanes 7–9). Finally, the mobility of the IGR transcripts

Downloaded from www.rnajournal.org on February 14, 2006

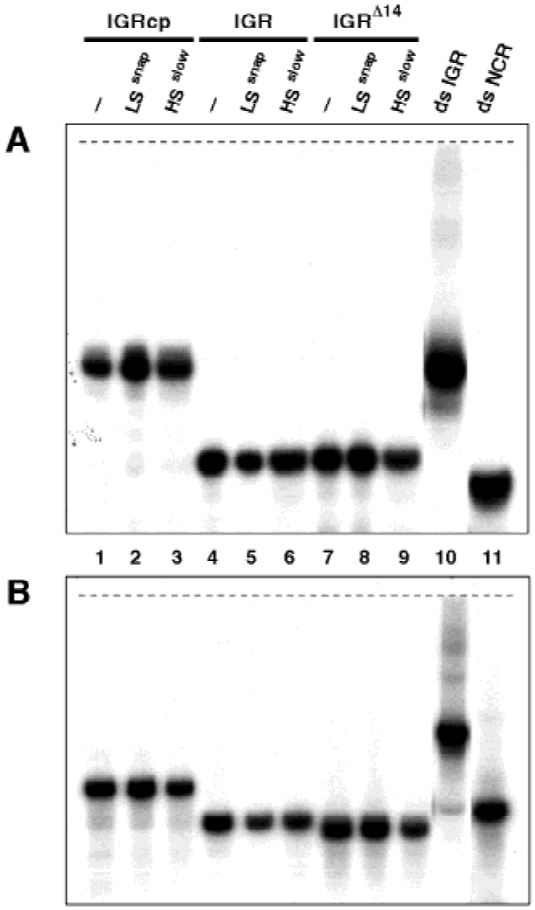

FIGURE 2. Analysis of transcripts covering the intergenic region (IGR) in nondenaturing gels. Aliquots of 5×10^4 cpm of each gel-purified transcript (IGRcp, IGR, IGR$^{\Delta 14}$) were pretreated in low salt buffer with EDTA (LS^{snap}), high salt buffer with $MgCl_2$ (HS^{slow}), or not pretreated (−) as described in Materials and Methods. Double-stranded RNAs provided as markers were prepared by annealing (+)- and (−)-strand transcripts covering the intergenic region (dsIGR) or the 5′-noncoding region (dsNCR) of RNA3. Horizontal electrophoresis was carried out for 3 h at 300 V in a 5% nondenaturing PAA gel (30:1) at 15 °C (18–20 °C in the gel) using 0.2×TBE (**A**) or 0.5×TBE and 5 mM $MgCl_2$ (**B**) as a buffer system. Gels were dried and exposed to X-ray film (NEN) for 6 h at room temperature. The dashed line indicates the position of wells where samples were loaded.

increased to some varying degree relative to two double-stranded RNAs (Fig. 2B, lanes 10, 11) when electrophoresis was carried out in 0.5×TBE with 5 mM Mg^{2+} (Fig. 2B), suggesting that the presence of magnesium induced a tightening of the IGR structure but no dramatic overall changes. The additional sequences present in IGRcp (Fig. 1) and their magnesium-dependent folding may in particular be responsible for the increased mobility of this transcript (Fig. 2A,B, lanes 1–3) relative to IGR and IGR$^{\Delta 14}$. Similarly, the deletion of 14 nt in IGR$^{\Delta 14}$ may render this transcript more dependent on magnesium to maintain its structure; hence the small increase in mobility observed relative to IGR (Fig. 2, lanes 4–9 in both panels). We cannot exclude that distributions of local structural alternatives are present that result in minimal hydrodynamic changes not resolved by this analysis. However, the possibility of such local differences can be best answered through the mapping experiments themselves.

In vitro structure mapping with CMCT and kethoxal

We probed the structure of selected RNA transcripts and RNA from in vivo sources by chemically modifying accessible bases with CMCT, kethoxal, DMS, and DEPC (Ehresmann et al., 1987, and references therein). Modified bases were identified by primer extension with reverse transcriptase, which detects methylation at the N3 position of uridines and N1 position of guanosines (CMCT), at N1 and N2 positions of guanosines (kethoxal), and at the N1 position of adenosines and N3 position of cytidines (DMS; Inoue & Cech, 1985). Where indicated, N7 methylation of guanosines (DMS) and N7 carboxylation of adenosines and guanosines (DEPC) were detected by primer extension after aniline-induced scission of the RNA strand (Peattie & Gilbert, 1980).

First, transcripts of full-length RNA3 and IGRcp (Fig. 1, top and middle) were treated with CMCT and kethoxal. This was done either in low salt buffer (50 mM cacodylate for CMCT or 50 mM borate for kethoxal) with 1 mM EDTA, referred to as semidenaturing conditions, or in the same buffer with medium salt (50 mM KCl) and 5 mM $MgCl_2$, which emulates native conditions (Ehresmann et al., 1987). Representative results are shown in Figure 3A (CMCT) and B (kethoxal). The same CMCT and kethoxal modification patterns were observed whether the IGR was presented in the context of the entire RNA3 (Fig. 3, lanes 1–6) or as an isolated transcript IGRcp (Fig. 3, lanes 7–12), implying a common IGR fold that is independent from the non-IGR sequences in RNA3. The majority of accessible bases were modified both under semidenaturing (Fig. 3, lanes 1–3, and 7–9) and native conditions (Fig. 3, lanes 4–6, and 10–12). This is in good agreement with the native gel electrophoresis results (Fig. 2) that implied similar overall structures in the presence and absence of Mg^{2+}. However, a few base positions were modified differentially under the two conditions. Where base accessibility was higher or occurred exclusively under semidenaturing conditions (open arrowheads in Fig. 3A,B), this may reflect local instabilities that require higher counterion concentrations and/or magnesium to remain base paired. On the other hand, some bases were modified with higher efficiency under native conditions (filled arrowheads), indicating sites of limited rearrangement between a low salt-EDTA and a medium salt-magnesium conformation.

Downloaded from www.rnajournal.org on February 14, 2006

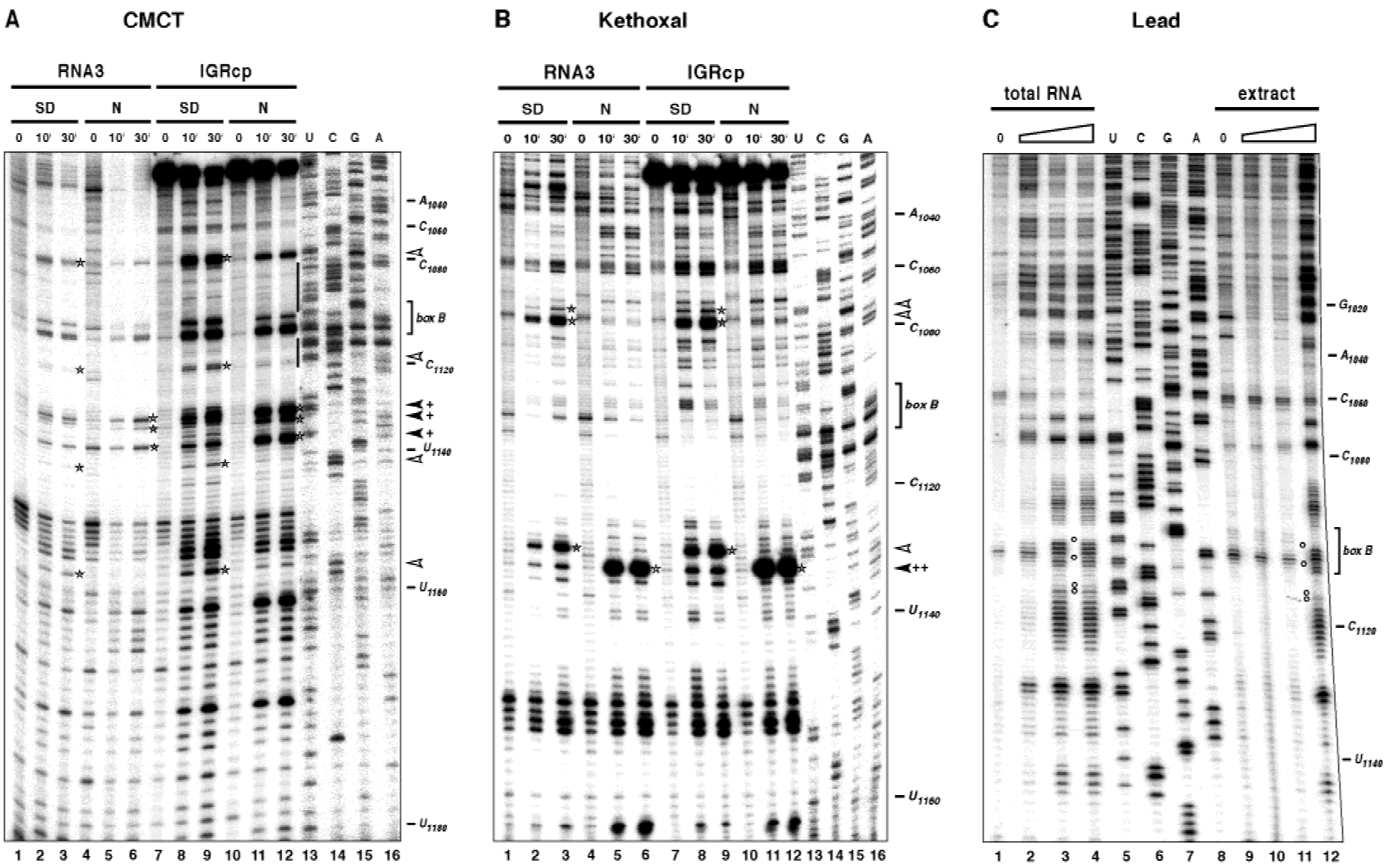

FIGURE 3. Chemical probing of the RNA3 intergenic region in vitro. **A,B:** Base modification with CMCT and kethoxal. In vitro transcripts of the entire RNA3 or IGRcp (see Fig. 1) were exposed to CMCT (**A**) or kethoxal (**B**) for 10 or 30 min (10′, 30′) under semidenaturing (SD) or native (N) conditions. Primer extension products of modified and unmodified (0) RNA were analyzed on denaturing PAA gels alongside DNA sequencing reactions (U, C, G, A). Note that the reverse transcriptase stops 1 nt 3′ to the modified base, creating an offset of one base between primer extension signals and corresponding bands in the sequencing lanes. Open arrows indicate base modifications that are more pronounced under semidenaturing conditions; filled arrows combined with "+" indicate stronger modification under native conditions; corresponding bands are marked by stars for easier identification within the gel. Bars between lanes 12 and 13 in **A** indicate uridine-rich regions flanking the box B element (bracket) that are significantly protected against CMCT modification under native conditions. **C:** Lead-induced cleavage of the ribose-phosphate backbone. Primer extension analysis of RNA3 expressed in vivo that had been exposed to increasing concentrations of lead acetate (wedge: 1 mM, 5 mM, 25 mM) in the context of purified total RNA from yeast (lanes 1–4) or in crude cellular extracts (lanes 9–12). 0: no-lead control; U, C, G, A: sequencing lanes. Open circles indicate the less accessible ribose moieties of U^{1102}, A^{1106}, U^{1112}, and U^{1113} discussed in the text. Sequence markers given to the right of these and all following panels point towards bands in the respective sequencing lanes, not necessarily the lane closest to the right.

Downloaded from www.rnajournal.org on February 14, 2006

In vitro and in vivo structure mapping with DMS and DEPC

To obtain information on the IGR structure in cells and cell extracts, we performed chemical modification with DMS, which permeates cell walls and membranes (Ares & Igel, 1990). Crude extracts of yeast cells expressing RNA3 in the presence or absence of coexpressed viral 1a protein (Fig. 4A) were used to probe the IGR structure together with cellular components. Additionally, whole cells expressing RNA3 ± 1a were exposed to DMS and then, as with the extracts, a total RNA preparation followed by primer extension was used to analyze the accessibility of adenines and cytosines (Fig. 4B).

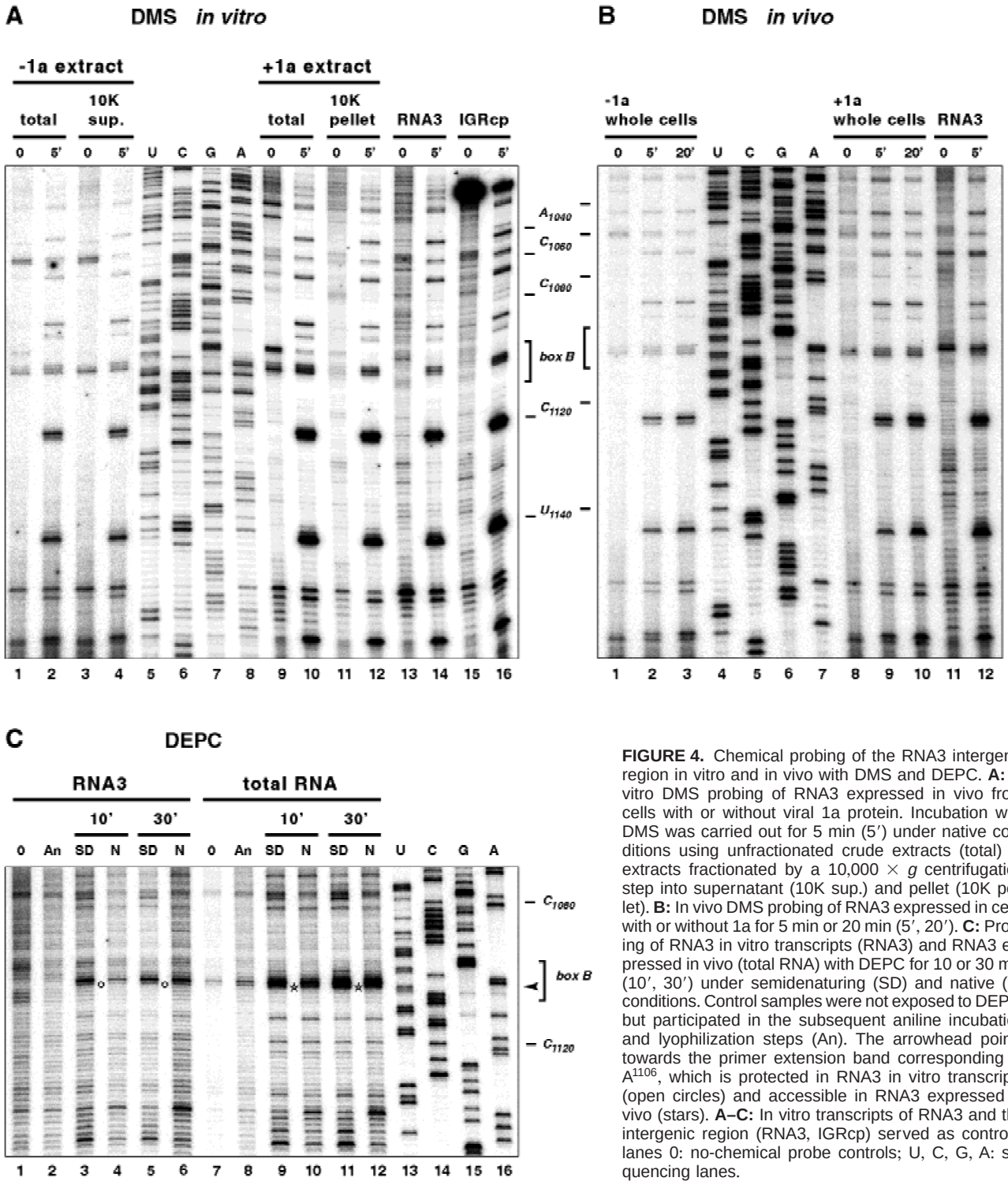

FIGURE 4. Chemical probing of the RNA3 intergenic region in vitro and in vivo with DMS and DEPC. **A:** In vitro DMS probing of RNA3 expressed in vivo from cells with or without viral 1a protein. Incubation with DMS was carried out for 5 min (5′) under native conditions using unfractionated crude extracts (total) or extracts fractionated by a 10,000 × *g* centrifugation step into supernatant (10K sup.) and pellet (10K pellet). **B:** In vivo DMS probing of RNA3 expressed in cells with or without 1a for 5 min or 20 min (5′, 20′). **C:** Probing of RNA3 in vitro transcripts (RNA3) and RNA3 expressed in vivo (total RNA) with DEPC for 10 or 30 min (10′, 30′) under semidenaturing (SD) and native (N) conditions. Control samples were not exposed to DEPC, but participated in the subsequent aniline incubation and lyophilization steps (An). The arrowhead points towards the primer extension band corresponding to A^{1106}, which is protected in RNA3 in vitro transcripts (open circles) and accessible in RNA3 expressed in vivo (stars). **A–C:** In vitro transcripts of RNA3 and the intergenic region (RNA3, IGRcp) served as controls; lanes 0: no-chemical probe controls; U, C, G, A: sequencing lanes.

Downloaded from www.rnajournal.org on February 14, 2006

As with CMCT and kethoxal, the majority of accessible bases could be modified under semidenaturing and native conditions (not shown). Furthermore, the same modification pattern was detected for the isolated IGR as well as the IGR in full-length RNA3 (Fig. 4A, lanes 14 and 16, and Fig. 4B, lane 12). This was also true for comparisons of purified, in vitro-transcribed RNA3 (Fig. 4A, lane 14, and 4B, lane 12) and in vivo transcribed RNA3 in cell extracts (Fig. 4A, lanes 2 and 10) or whole cells (Fig. 4B, lanes 2,3 and 9,10). Taken together, these results provided no indication for site-specific, stable protection by proteins. Similarly, the presence or absence of viral 1a protein did not change the modification pattern in whole cells (Fig. 4B, lanes 2,3 vs. 9,10) or crude extracts (Fig. 4A, lane 2 vs. 10). As noted earlier, 1a mediates RE-dependent stabilization of RNA3 and directs RNA3 to the membrane-associated BMV RNA replication complex (Sullivan & Ahlquist, 1999; Chen et al., 2001; M. Janda & M. Sullivan, unpubl. results). This was reflected in the comparison of yeast extracts without 1a, where the majority of RNA3 was found in the supernatant of a 10,000 $\times$ *g* centrifugation (Fig. 4A, compare lanes 1,2 with 3,4), and extracts including 1a, where the majority of RNA3 was recovered in the membrane-rich pellet of such a fractionation (Fig. 4A, lanes 9,10 vs. 11,12). Again, there was no detectable effect on the IGR structure of relocalizing RNA3 from the cytoplasm (Fig. 4A, lane 4) to the replication complex on the ER membrane (Fig. 4A, lane 12).

When we used DEPC carboxylation to probe accessibilities of adenines at the N7-Hoogsteen position we found largely the same pattern of modification as with DMS (Fig. 4C). Again, RNA3 in vitro transcripts and RNA3 derived from in vivo appeared highly similar with one particularly notable exception (marked by an arrowhead): For in vitro transcripts, only one of the two adenines in the box B element, A_{1105}, showed significant modification with DEPC, whereas A_{1106} remained strongly protected (Fig. 4C, open circles, lanes 3–6). However, when total RNA from yeast cells expressing RNA3 was used, both adenines were widely accessible (Fig. 4C, stars, lanes 9–12). The implications of this difference are discussed further below. In addition to this major change, a few minor differences between in vitro transcripts and in vivo RNA were found under semidenaturing conditions (Fig. 4C, lanes 5 and 11, near bottom), although the significance of these is unclear because they were not reproduced under native conditions (Fig. 4C, lanes 6 and 12).

RE forms an extended secondary structure ending in a TΨC-stem loop

As a starting point for structural modeling of the RE, the folding potential of the entire BMV RNA3 sequence was examined with the program *mfold 3.0* (Mathews et al., 1999; Zuker et al., 1999), generating a hierarchy of alternate RNA3 structures with increasing free energies. The top 5% of these predictions (see Materials and Methods) contain the IGR sequence encompassing the RE folded back onto itself. Among the resulting RE structures, maximum correlation with the chemical modification data was found with a conformation (Fig. 5A,C) closely related to the structure of predicted lowest free energy. This structure and the predicted lowest free energy structure were identical over most of the RE and in these regions showed good matching with the modification results. However, the two structures differed in base pairing in a single internal segment encompassing nt 1065–1091 and 1119–1141 (Fig. 5A,B). In this region, the structure of predicted lowest free energy (Fig. 5B) failed to explain the accessibility of bases U_{1128} to A_{1133} to CMCT, kethoxal and DMS in semidenaturing conditions or, under native conditions, the accessibility of residues U_{1130} and G_{1132} to CMCT and kethoxal. In contrast, the alternate conformation in Figure 5A,C placed all of these accessible bases in a large 19-nt internal loop or at the border of helices.

This 19-nt loop region contained the sites with the greatest accessibility differences between semidenaturing and native conditions (Fig. 5A,C). Accordingly, although this structure closely matched the modification data under semidenaturing conditions (Fig. 5A), it did not immediately explain the inaccessibility under native conditions of a few residues within nt 1072–1080 (Fig. 5C). Because the IGR structure was unaffected by the presence or absence of the remaining RNA3 sequences, any interactions protecting these residues must be within the IGR. The good fit of the mapping data in all other respects as well as the lack of any major conformational shift between semidenaturing and native conditions (Fig. 2) suggests that this protection may arise from non-Watson–Crick (WC) interactions, possibly within the loop itself.

One side of the large 19-nt loop, oriented towards the bottom of the RE structure (to the left in Fig. 5), is stabilized by a helical segment with six G:C base pairs (nt 1060–1066 and 1143–1149), flanked by three internal loops and one bulge loop separated by helices. All four loops were well accessible to modifying agents; the absence of modification data for U_{1179} and U_{1180} (Fig. 5) resulted from primer extension oligo OL4 binding just 2 nt away and the inability of reverse transcriptase to read efficiently and in register across the oligo-A tract from further downstream primers like OL5 (Fig. 1). Overall, the modification results well support the indicated arrangement of conventional loops and double-stranded helices.

On the other side of the 19 nt loop, towards the tip of the structure (to the right in Fig. 5), are several short, 2-bp helices setting up one bulge and three internal loops. Three of these loops were significantly less accessible to base modification than the other loops discussed so far, prompting us to further investigate the

Downloaded from www.rnajournal.org on February 14, 2006

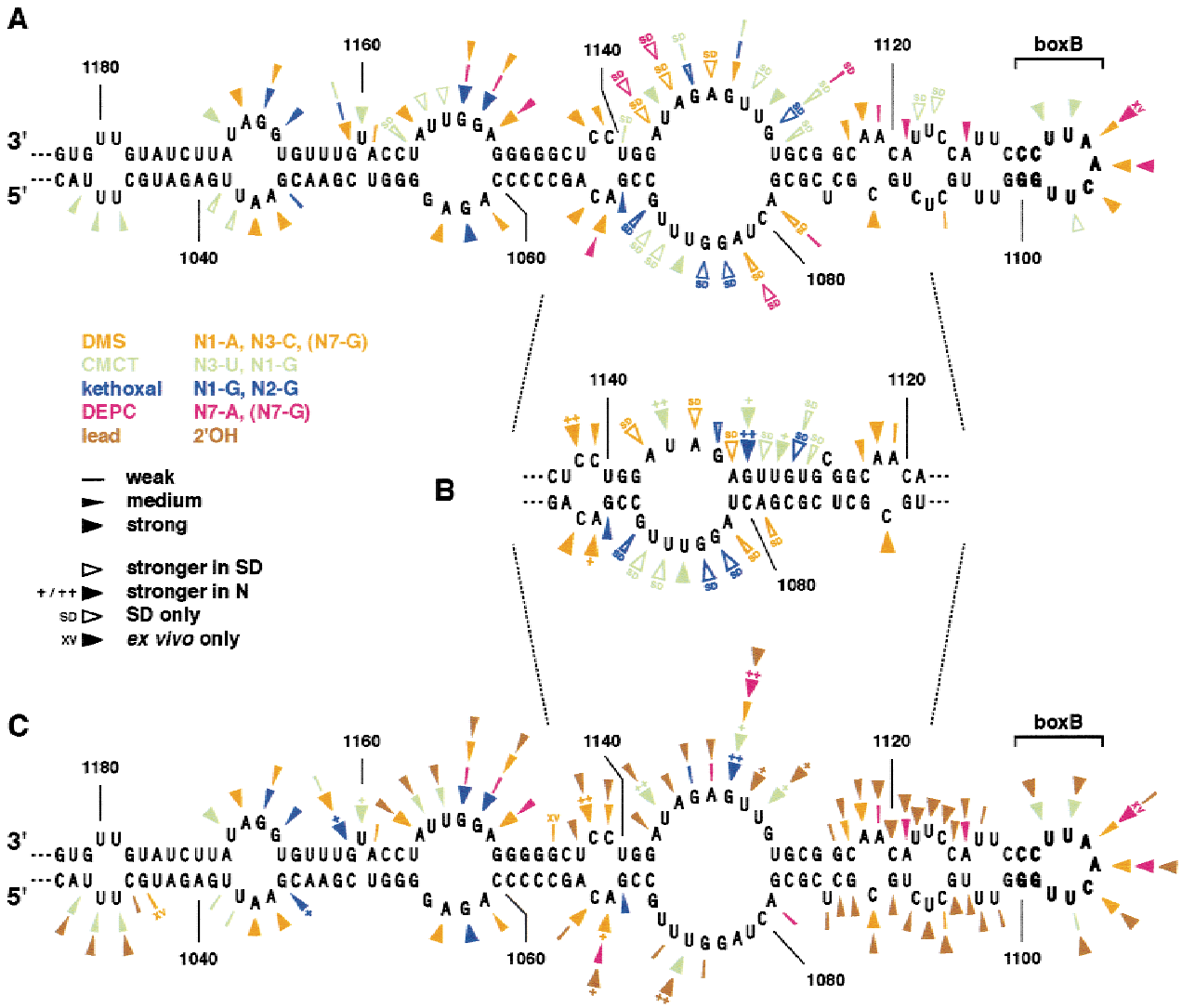

FIGURE 5. Secondary structure model of the intergenic replication enhancer, RE. Modification results obtained under semidenaturing (**A**) and native (**C**) conditions are shown superimposed over the secondary structure that best fit all mapping data. **B:** Segment from the secondary structure with calculated lowest free energy in the region where it differs from the structure best satisfying the experimental constraints (**A,C**). Outside the segment shown here, both structures have the identical base pairing and loops. A subset of the mapping data from **A** and **C** are shown superimposed over the structural detail (**B**). Note how a number of accessibilities between U^{1128} and A^{1133} in the upper strand conflict with the helical element predicted in the structure of calculated lowest free energy.

nature of this region with lead-induced cleavage of the ribose-phosphate backbone. The results, shown in Figure 3C and summarized in Figure 5C, are discussed below together with additional phylogenetic data.

Finally, at the tip of the structure, the box B sequence is presented as a hairpin loop of 7 nt closed by three G:C base pairs. Unlike the internal loops in the left half of the structure, the box B loop nucleotides were not equally accessible to modification. U_{1102} showed no modification with CMCT and no lead induced cleavage. U_{1103}, C_{1104}, and A_{1105} were all accessible to lead, yet U_{1103} was modified by CMCT much more strongly under semidenaturing conditions than the other two were by DMS (A and C) or DEPC (A). A_{1106} showed much lower accessibility to lead than the surrounding nucleotides (Fig. 5C), in contrast to good DMS modification. U_{1107} and U_{1108} were well accessible to lead and CMCT, with U_{1108} being particularly accessible under native conditions. As discussed further below, the box B consensus sequence (Fig. 1, bottom), its folding pattern, and the observed accessibilities of the loop nucleotides are all highly reminiscent of the TΨC-stem loop in tRNA, raising the question of further structural and possible functional similarities.

Downloaded from www.rnajournal.org on February 14, 2006

BMV RNA3 is modified within the box B element in vivo

The significantly different modification behavior of A_{1106} in in vivo versus in vitro-synthesized RNAs led us to more closely examine the immediate environment of this nucleotide. In tRNA, the corresponding loop is nearly always modified posttranscriptionally, yielding a riboT (= 5^mU) at tRNA position 54, a pseudouridine (Ψ) at position 55 and frequently a 1^mA at position 58 (Sprinzl et al., 1998). X-ray studies show that, in tRNA, these modified nucleotides are critically involved in tertiary interactions across the TΨC loop and between the TΨC and D loops (Dirheimer et al., 1995, and references therein), with the T-modification alone contributing a 6 °C increase in T_m value of the tRNA (Davanloo et al., 1979). Although the exact function of these modifications are not known, evidence from systems with un- and undermodified tRNAs suggests that the modifications' contribution to the correct three-dimensional architecture of tRNA may have an influence on correct aminoacylation, translation accuracy, and ribosomal A-site binding (Perret et al., 1990a; Björk, 1992).

T and Ψ modifications in RNA can be probed by chemical modification and detected by primer extension (Bakin & Ofengand, 1993). To assay for possible Ψ modification, we incubated in vitro transcribed RNA3, total RNA from yeast expressing RNA3 + 1a protein, and BMV virion RNA from infected barley plants (Lane, 1986) with CMCT under denaturing conditions. CMCT modifies all uridine derivatives to varying but detectable extents. Subsequent mild alkaline treatment removes the bulky CMCT adduct from U and T, but leaves it bound to Ψ, resulting in a strong stop in primer extension (Bakin & Ofengand, 1993). As shown in Figure 6A, such a strong stop band (marked by an arrowhead) is found at U_{1103} after probing RNA3 from yeast cells (lane 8, star) or virion RNA3 from BMV-infected barley plants (lane 16, star), but not in vitro-transcribed RNA3 (lane 4, open circle). The same Ψ modification can be detected in RNA3 from cells not expressing viral 1a protein (not shown). We conclude that in both plant cells and yeast, a large fraction of RNA3 IGR is modified to yield Ψ at position 1103, corresponding to tRNA Ψ_{55}.

To assay for T modification, we modified uridines with hydrazine and then cleaved the RNA chain with aniline (Bakin & Ofengand, 1993). In contrast to regular U, T and Ψ are not efficiently modified by hydrazine, so that primer extension results in stops at U and read-through

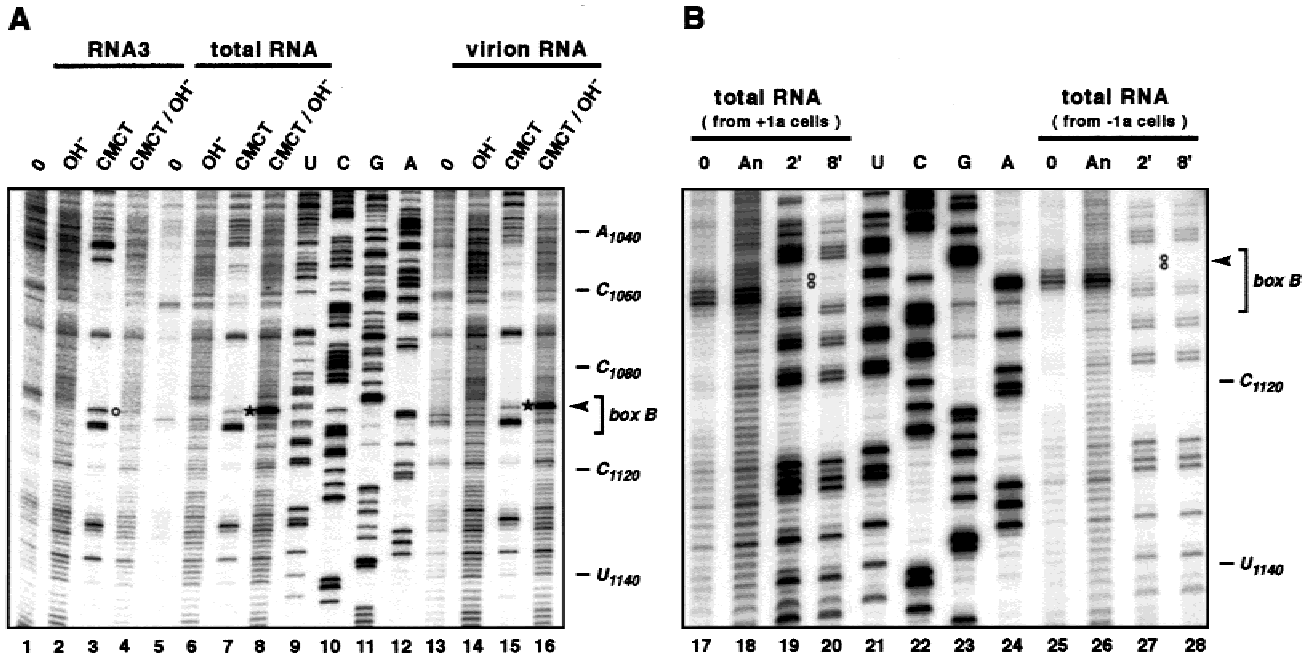

FIGURE 6. Detection of T and Ψ modifications within the RE. **A:** Analysis of Ψ modifications in the RE of RNA3 from in vitro transcription (RNA3), expression in yeast (total RNA) and virus replication in barley plants (virion RNA). Before primer extension, samples were modified at uridine residues by incubation with CMCT and then treated with mild alkaline buffer to remove CMCT from all U-variants but Ψ (lanes CMCT/OH^-). The arrowhead points to the band corresponding to U^{1103}, which gives rise to a strong primer extension stop in RNA3 from in vivo sources (marked by a star), but no detectable signal in RNA transcripts (open circle). Controls include untreated RNA (0), RNA modified chemically only (CMCT) and RNA treated with mild alkali only (OH^-). **B:** Analysis of T and Ψ modifications in the RE of RNA3 expressed in yeast. Samples were treated with hydrazine for 2 or 8 min and then underwent aniline scission (lanes 2′, 8′). Note the absence of bands (open circles, arrowhead on the right) corresponding to U^{1102} and U^{1103} in comparison to other U residues below and above generating primer extension stops. Controls include untreated RNA (0) and RNA treated with aniline only (An); U, C, G, A: sequencing lanes.

Downloaded from www.rnajournal.org on February 14, 2006

at T and Ψ. When we subjected total RNA from yeast expressing RNA3 with or without 1a to this procedure, both positions in question, U_{1102} and U_{1103} (Fig. 6B, arrowhead), were resistant to cleavage (Fig. 6B, open circles in lanes 19, 20, 27, and 28). In combination with the results from CMCT + alkali, this confirms the Ψ modification at U_{1103} and shows that U_{1102} bears a different modification. Because, with the exception of Ψ and T, all other known in vivo modifications of uridine have been reported to be receptive to hydrazine–aniline cleavage (Lankat-Buttgereit et al., 1987), we therefore conclude that the nucleotide at position 1102 is a T. When the more varied box B element at the 5′ end of RNA3 (Fig. 1) was probed with both assays, no uridine modifications could be detected. Similarly, a stretch of single-stranded nucleotides within the conserved tRNA-like 3′ end of RNA3, which has been proposed to correspond to the T-loop (Felden et al., 1994), was tested for U modifications. As for the 5′ end, none were observed (not shown).

The pyrimidine-rich region adjacent to box B adopts an unconventional structure

One unexpected result from the CMCT mapping experiments was a lack of significant U modification in the sequences immediately flanking the box B element (nt 1091–1098 and 1112–1118), particularly under native conditions (Fig. 3A, compare lane 12 to lane 13 at the sequence denoted by bars; see also Fig. 5). This contrasted with computer predictions placing these residues in internal and bulge loops (Fig. 5), a state normally associated with accessibility to chemical modification.

To investigate this, we probed the IGR structure with lead, which attacks solvent-exposed ribose moieties (i.e., in single-stranded or loop regions) at the 2′-OH, leading to hydrolysis of the 3′-phosphodiester bond (Farkas, 1968; Brown et al., 1983). Lead probing was performed on total RNA extracts from cells expressing RNA3 and 1a or on crude extracts from the same cells. As shown in a representative example (Fig. 3C), the presence of proteins in whole-cell extracts (lanes 10–12) required higher lead concentrations than purified total RNA preparations (lanes 2–4) to achieve the same level of cleavage. However, the same overall cleavage pattern was obtained in both cases (Fig. 3C, compare lanes 4 and 12), confirming results from DMS modification in cell extracts and in vivo (Fig. 4), where also no evidence for a stable protein footprint or protein-induced conformational change could be detected. No particular lead cleavage site stood out at low lead concentrations, indicating no evidence for a specific metal ion binding site, which is a common signature of tertiary structure formation (Misra & Draper, 1999; Tinoco & Bustamante, 1999). Again, this is in good agreement with base modification data (Fig. 3A,B; Fig. 4A,B) which did not show differences between isolated IGR and RNA3 transcripts; such differences might have been expected for tertiary interactions involving IGR and non-IGR secondary structure elements.

In general, accessibility to lead paralleled accessibility to CMCT, kethoxal, or DMS (Fig. 5). In particular, partial protection from lead cleavage was found for $U_{1097}U_{1098}$ and particularly $U_{1112}U_{1113}$ flanking the box B sequence as well as U_{1102} and A_{1106} within box B (Fig. 3C, open circles), confirming results with CMCT (Fig. 3A), DMS (Fig. 4A,B), and DEPC (Fig. 4C). The protection and inferred structuring of the UU sequences immediately flanking the predicted 3-bp box B stem in Figure 5C is strongly supported by the observed in vivo modification of U_{1102} to T = 5^mU, as host tRNA 5^mU methyltransferase (RUMT) only recognizes T-stem loop substrates with stems of at least 5 bp (Becker et al., 1997). Consequently, the flanking UU sequences may be involved in tandem U:U pairs as found previously in other RNAs (Nagaswamy et al., 2000).

Adjacent to this double-UU opposition are two internal loops and one bulge separated by 2-bp helices (nt 1087–1096 and 1114–1122). This region was highly prone to lead-induced cleavage (Fig. 5C), which could indicate instability and a high proportion of molecules in which this region is single stranded. However, when base modification data are taken into account, a more complex picture emerges. For example, in the predicted third loop (CUC/CUU) from the tip of the IGR structure, one C showed little modification by DMS, two U residues received CMCT modification only under semidenaturing conditions, and three residues were not modified at all (Fig. 5A). Similarly, the 2-bp helices flanking this loop showed DEPC modification of adenines at the N7- or Hoogsteen position of the base, but no WC modifications, implying that these nucleotides are not in a simple single-stranded conformation. Thus, in this region, many residues were either little modifiable or were overall undermodified in comparison to their accessibility by lead, indicating a structure not composed of standard A-type helices, but one where the backbone is distorted and thus the ribose moieties become exposed, yet where the bases are involved in base pairing and/or stacking interactions that impede modification.

Conservation of a tRNA-like structure among *Bromoviridae*

Conserved box B sequences are found not only in BMV and other members of the bromovirus genus, but also in the cucumoviruses, which comprise a distinct genus in the *Bromoviridae* family, differentiated by many significant features (van Regenmortel et al., 2000). RNA3 from the cucumoviruses cucumber mosaic virus (CMV), tomato aspermy virus (TAV), and peanut stunt virus (PSV), for instance, all contain a fully conserved box B element in their IGR (Davies & Symons, 1988; Karasawa

Downloaded from www.rnajournal.org on February 14, 2006

et al., 1991; O'Reilly et al., 1991). Moreover, as for BMV, CMV IGR sequences containing the box B are required *in cis* for efficient RNA3 replication (Boccard & Baulcombe, 1993).

Accordingly, we explored whether the sequences surrounding the fully conserved intergenic box B elements in cucumovirus RNA3s showed any similarities to the BMV RNA3 RE and its structure. Using the program ConStruct (Lück et al., 1999), we aligned the complete RNA3 IGR sequences from 13 CMV subgroup I strains and 5 subgroup II strains, 5 strains of TAV, and 3 strains of PSV and compared the result with the BMV IGR. For clarity, the resulting alignment is depicted in Figure 7A for the area surrounding the box B element and including one representative of each cucumovirus subgroup. In addition to an identical box B element, each of these viruses extended the closing G:C base pair into a conserved helix of 3 to 4 bp, thus forming a tRNA-like TΨC-stem loop (Fig. 7B, bold face). According to the ConStruct algorithm, this was the most highly conserved part of the IGR consensus structure (Fig. 7A, helix "t" in orange). Also the next helix ("s" in dark yellow) was structurally well conserved. Notably, between helices "s" and "t," a predicted oligo-U loop was conserved with slight variations in size from four uridines in BMV to seven Us in PSV (bold dotted lines in Fig. 7B). Following helix "s," the pyrimidine-rich internal loop found to be much less accessible to base modifications than to lead cleavage in BMV (compare Fig. 5) was matched by similar pyrimidine-rich loops in the other viruses (Fig. 7B, thin dotted lines). The further distal from the TΨC-stem loop along the consensus IGR structure, the less the structural elements were conserved (light yellow to white in Fig. 7A) until eventually each virus group folded the 5′ and 3′ parts of its IGR sequence (beyond the alignment segment shown) into a distinct conformation.

DISCUSSION

In this study, we examined the structure of the BMV RNA3 replication enhancer, a crucial RNA replication signal through which BMV 1a protein recognizes RNA3 and recruits it from translation to RNA replication (Janda & Ahlquist, 1998; Sullivan & Ahlquist, 1999). As shown above, base modification, lead cleavage, secondary structure calculations, and phylogenetic conservation all indicate that the RE and flanking intergenic sequences adopt an unbranched, extended secondary structure. In this the RE folds back onto itself to present the conserved box B stem loop in a tRNA-like TΨC-loop at the end of an elongated stem punctuated by internal and bulge loops (Figs. 5 and 8). Not only the box B stem loop but several structural elements adjacent to it, including opposed oligo-U sequences and a pyrimidine-rich loop spaced by short helices, were conserved in the RNA3s of varied members of the *Bromoviridae* (Fig. 7). As discussed further below, the box B stem loop displays extremely close sequence and structural mimicry of a tRNA TΨC-loop, allowing it to be recognized in vivo by at least two tRNA-specific host enzymes, which efficiently modify two specific U residues to T and Ψ (Fig. 6).

Thus, we find that both of the first two steps of BMV RNA replication, template selection at the intergenic RE and initiation of negative-strand RNA synthesis at the aminoacylatable 3′ end, are directed by signals recognized by host, tRNA-specific enzymes. The use of tRNA-like elements in both of these steps could reflect the need to coregulate translation and replication of the same RNA (Janda & Ahlquist, 1998). Moreover, interaction between tRNA-specific factors bound to both sites might facilitate the transition from replication complex recognition at the RE to initiation at the distal 3′ end. In this context, our finding that the RE, but not the 3′ end, is recognized for T and Ψ modification suggests that these two regions might mimic complementary rather than redundant features of tRNAs.

The self-contained folding of the RE (Figs. 5 and 8) is consistent with its ability to act as an independent functional module, making nonviral RNAs fully responsive to 1a-mediated stabilization (Sullivan & Ahlquist, 1999). The boundaries defining the minimal RE further support this correlation: maximal 5′ and 3′ deletions retaining RE function (Sullivan & Ahlquist, 1999) have their endpoints within the same internal loop in the IGR secondary structure (Fig. 8, filled arrows), consistent with the RE as a structural unit beyond simple sequence requirements. Because the next two deletions (open arrows) fail to support 1a-mediated RNA stabilization and replication, the intervening segment may constitute a functional RE subdomain. Alternatively, this segment may have a more indirect role such as stabilizing the conformation of recognition elements closer to the apical box B stem loop (further to the right in Fig. 8). Although the central part of the IGR containing the RE was mapped most rigorously (Fig. 5), DMS, CMCT, and kethoxal modification analysis using primers OL2 and OL5 (Fig. 1) and computer-predicted folding of the entire RNA3 sequence support the complete IGR structure in Figure 8, in which the flanking intergenic sequences extend the rod-like RE structure with little or no contribution from the surrounding 3a and coat protein ORFs.

Structure probing under a variety of conditions, including with in vitro transcripts under different salt and magnesium concentrations and with in vivo transcripts in crude yeast extracts and in whole cells, indicated that the deduced structure predominated in vitro or in vivo, with little or no representation of alternate folds in the RNA3 population. This is in good agreement with the migration of IGR transcripts in native gels (Fig. 2), where only one major band was detected no matter

Downloaded from www.rnajournal.org on February 14, 2006

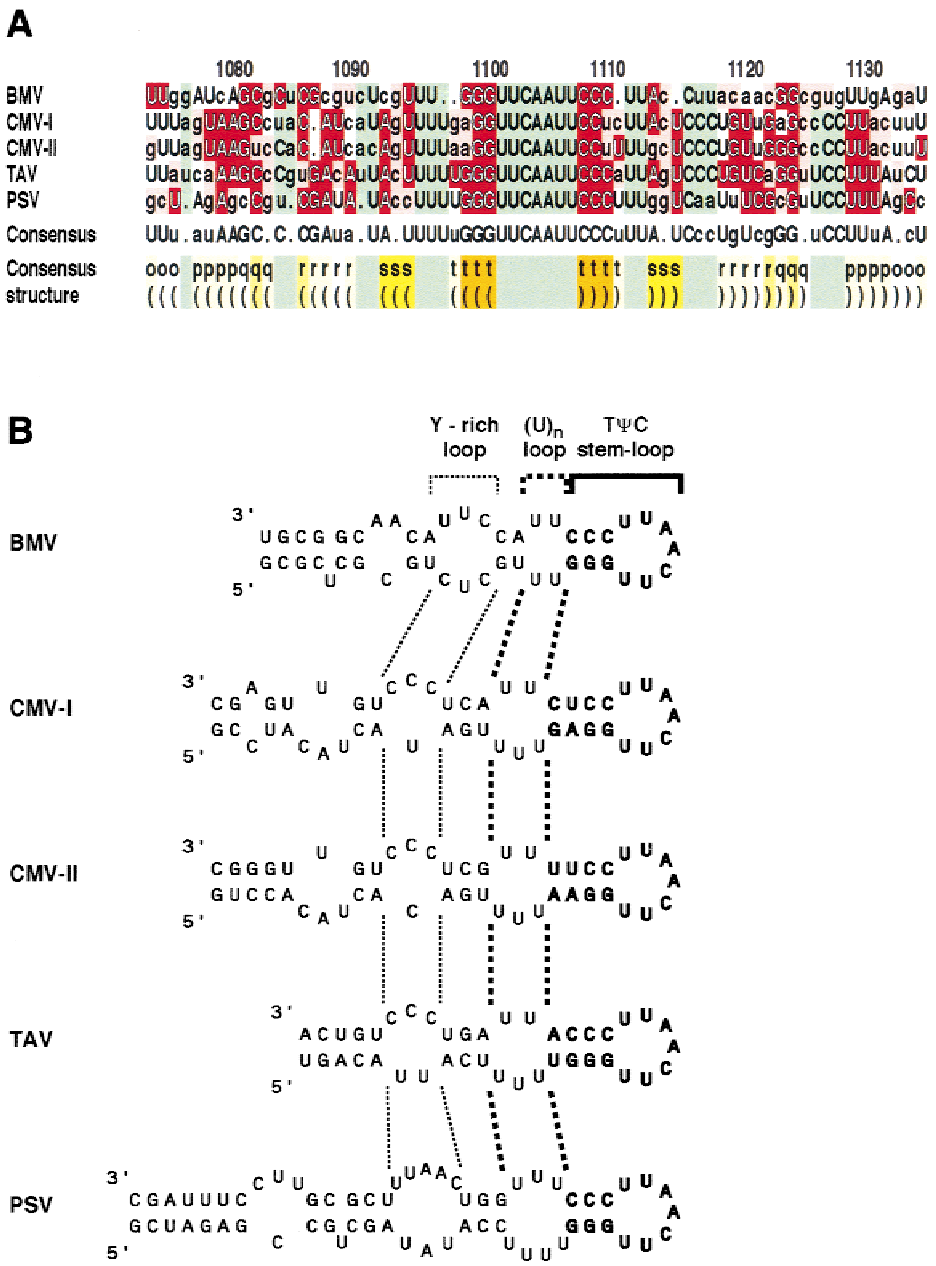

FIGURE 7. Conservation of structure between BMV and cucumoviruses. **A:** Detail from a structural alignment performed on IGR sequences from BMV, CMV subgroups I and II, TAV, and PSV using ConStruct (Lück et al., 1999). Nucleotides predicted to base pair are color coded red to denote a match to the consensus sequence or pink to designate compensatory changes preserving the base pair; nucleotides predicted unpaired are green, and white nucleotides contradict a consensus base pair. In the line labeled "consensus," a capital letter is given for a conservation of an absolute majority (here: ≥2.5) of sequences and a small letter for conservation in a relative majority (here: 2) of sequences; a dot designates no clear conservation or a 1:1 split between 2 nt. Note that in assigning this consensus, each of the two CMV sequences is attributed only half the weight of any other sequence (e.g., first column on the left "U-U-g-U-g" is counted as 2.5 Us and 1.5 Gs, resulting in a capital letter U for the consensus sequence, whereas the third column "g-U-U-a-U" is counted as two uridines total, resulting in the small-letter u for the consensus sequence). In the two lines labeled "Consensus structure" helix formation is marked by brackets and individual helices are denoted by small characters; increasing base pairing probabilities are shown by deepening color code from white over shades of yellow to orange. The numbering given in the first line refers to the BMV RNA3 sequence as used throughout this paper. **B:** Conserved part of the IGR secondary structures of BMV and cucumoviruses as predicted by ConStruct. The decreasing conservation of elements from the TΨC-stem loop (bold nucleotides) to the uridine-rich loop $(U)_n$ and the pyrimidine(Y)-rich loop is indicated by a bold bracket and thick or thin dashed lines and brackets, respectively.

how transcripts were pretreated. Thus, we expect this RE structure to be the one to interact with proteins, cellular and/or viral, for at least the initial step(s) of recruitment into the replication complex. The relatively large size of the active RE (Sullivan & Ahlquist, 1999) and our finding that structural features beyond the

Downloaded from www.rnajournal.org on February 14, 2006

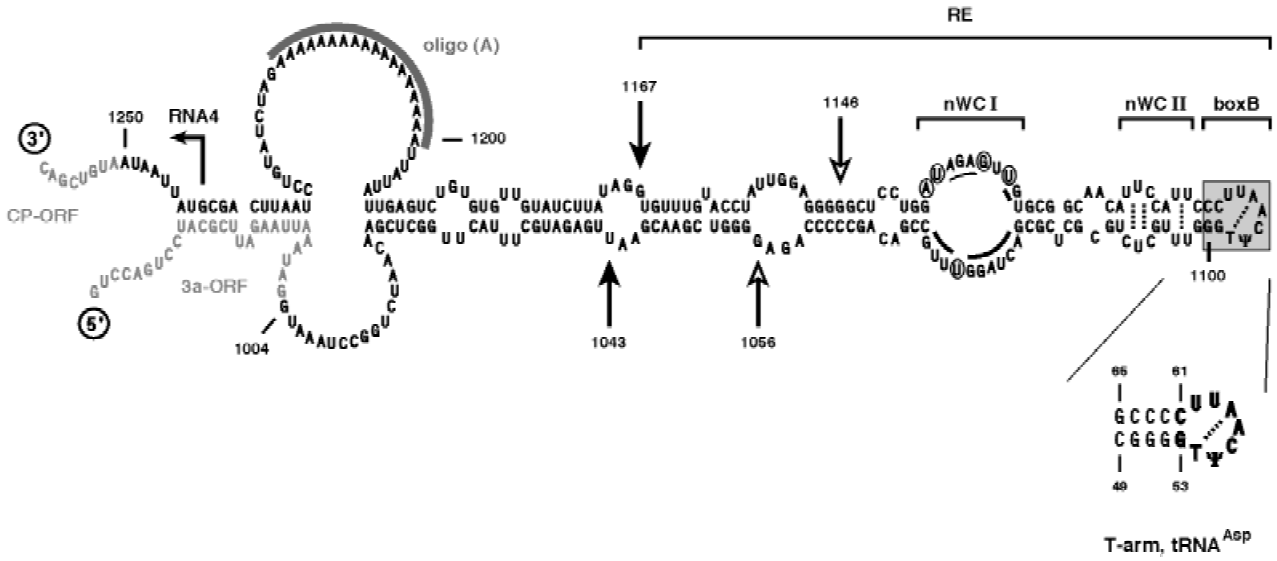

FIGURE 8. Secondary structure model of the entire IGR. Folding of the IGR sequence (black letters, nt 1004–1250) and flanking open reading frames for the 3a and coat protein (gray letters) summarizes results from this work and others discussed in the text. Start site for subgenomic RNA4 synthesis and the oligo-A tract are designated by a bracketed arrow and a grey bar. The intergenic replication enhancer (RE) was characterized by earlier deletion studies (Sullivan & Ahlquist, 1999) defining maximum 5′ and 3′ deletions that were still functional (filled arrows) as well as further deletions that lost biological activity (open arrows). Areas of possible non-WC base pairing are indicated by brackets (nWCI, nWCII, boxB); nucleotides in nWCI that were highly accessible to chemical probes under native conditions are circled, weakly or strongly protected nucleotides are marked by thin or thick curved bars; possible U:U and U:C interactions across the predicted loops in nWCII that would lead to the observed protection (see Fig. 5) are indicated by dashed lines. The conserved box B element (gray box) carries the T and Ψ modification made in vivo (Fig. 6). To highlight the extraordinary tRNA mimicry, the T-arm from $tRNA^{Asp}$ (conserved nucleotides in bold face) is shown below; the dashed lines represent the reverse Hoogsteen base pair between T and A discussed in the text.

TΨC-stem loop are conserved (Fig. 7) are suggestive of more than one binding protein site, indicating an interaction that may be complex. Our determination of the RE structure will thus facilitate design and interpretation of protein interaction studies with this region.

Features of the RE structure

Three regions of unusual structure and potential noncanonical base interactions were identified within the RE structure. One was the 19-nt predicted loop region (nWC I in Fig. 8). Although most bases in this loop were accessible to modification under low salt conditions (Fig. 5A), conditions closer to those in vivo, with millimolar magnesium and medium salt (Fig. 5C), exposed some nucleotides (circled in Fig. 8) strongly to the solvent whereas adjacent residues (curved bars in Fig. 8) were highly protected from base modification, lead cleavage, or both. A second region (nWC II in Fig. 8) contained a loop of six pyrimidines and opposed UU sequences whose nucleosides were either accessible to lead cleavage at the ribose moieties but fairly protected at the bases (Pyr_6) or hardly accessible at all (U_4). These results are consistent with the possibility of U:U, tandem-U:U, or U:C non-WC interactions (dotted lines in nWC II) found in other biological examples like ribosomal RNA (Wang et al., 1996), a hammer-head ribozyme (Simorre et al., 1997), or a tetraloop receptor (Butcher et al., 1997). Such regions, where the RNA structure deviates from standard A-type helix and local backbone distortions expose particular nucleosides towards the solvent, are prime candidates for specific recognition by proteins (Draper, 1999; Hermann & Patel, 2000).

The third region of unusual structure was the box B element itself, which is presented at the tip of the RE structure in a conformation closely mimicking the TΨC-stem loop of tRNAs (Fig. 8). While tertiary interactions between the D- and TΨC-loop help orchestrate the network of contacts in tRNAs (reviewed by Saenger, 1984), studies on tRNAs and tRNA subdomains (Westhof et al., 1983, 1985; Romby et al., 1987b; Yao et al., 1997; Koshlap et al., 1999) show that the TΨC stem loop alone forms a conserved structure recognized by the cellular proteins that modify tRNA nt U_{54}, U_{55}, and A_{58}. According to the substrate requirements of these enzymes in *Escherichia coli* (Gu & Santi, 1991; Gu et al., 1998), *Xenopus* (Grosjean et al., 1996), *Tetrahymena* (Sengupta et al., 2000), and yeast (Becker et al., 1997) and supported by phylogenetic comparisons (Sprinzl et al., 1998), the key identity determinants and features of the TΨC-stem loop structure (Fig. 8, detail) are: (1) a 7-nt loop of more or less strin-

Downloaded from www.rnajournal.org on February 14, 2006

gently conserved sequence (see Fig. 1) closed by the base pair G53:C61; (2) a stem of at least 3–4 bp for formation of Ψ_{55} by pseudouridine synthase and at least 5 bp for methylation of U_{54} by tRNA 5^mU methyltransferase (RUMT), with the second base pair from the loop preferably Pur_{52}:Pyr_{62}; (3) U_{54} and A_{58} form a reverse Hoogsteen base pair (dotted line in Fig. 8) that stacks on the loop-closing G:C ; and (4) N_{59} and Pyr_{60} are bulged out from the loop with the phosphate P_{60} involved in stabilizing hydrogen bonds to C_{61} and the ribose of A_{58}.

Our model of the box B sequence within the RE structure (Fig. 8, shaded box) shares these characteristics with only minor differences. Matches to the identical and conserved sequences in the 7-nt box B T-loop, the closing G:C base pair and 3 bp G:C stem, which are sufficient for recognition by host pseudouridine synthase (Becker et al., 1997), result in efficient in vivo modification of IGR U_{1103} to yield Ψ (Fig. 6). Additionally, we found efficient 5^mU modification of U_{1102}, presumably by host RUMT (Fig. 6). This result was intriguing because RNA substrate recognition by RUMT requires a T-loop stem of at least 5 bp (Becker et al., 1997), whereas the RE sequence predicts only 3 WC base pairs in the stem immediately adjacent to box B (Fig. 8). This underscores our finding that the adjacent double-UU loop may actually be base paired, thus elongating the G:C helix sufficiently to satisfy the requirement for the proposed recognition by RUMT.

The accessibility of U/Ψ_{1103}, C_{1104}, A_{1105}, U_{1107}, and U_{1108} to chemical modification are all in agreement with a TΨC-loop structure in the absence of a D-loop interaction (Romby et al., 1987b). Furthermore, the strong protection of U/T_{1102} and A_{1106} argue for the potential to form the reverse Hoogsteen base pair found in tRNA. In particular the protection of the N7 position of A, which should be involved in a hydrogen bond with U, against DEPC, when in vitro transcripts were probed (Fig. 4), supports this model. A point mutation ($A_{1106} > G$) within box B that reduces replication levels of RNA3 in barley plants by 50% (Smirnyagina et al., 1994) would inhibit the formation of the reverse Hoogsteen base pair across the loop (Fig. 8, dotted line), further emphasizing the apparent pressure to maintain the TΨC-stem loop structure in detail for biological function.

However, the TΨC-stem loop without stabilizing D-loop interactions is less rigid in its structure (Grosjean et al., 1998). The U:A reverse Hoogsteen base pair in particular is easily perturbed by changes in the local environment as shown by studies on isolated T-arms reporting a weakened U_{54}:A_{58} base pair (Louise-May et al., 1996) or T_{54} and A_{58} protection by stacking on the closing G:C, but not forming a base pair (Koshlap et al., 1999), and yet another study revealed an even higher degree of flexibility within the loop and no proximity between U_{54} and A_{58} at all (Yao et al., 1997; Schmitz et al., 1998). The in vivo modifications T_{1102} and Ψ_{1103} found in the BMV RE may induce a similar disturbance in the T_{1102}:A_{1106} geometry by their strong base stacking potential (Davis, 1995; Wang & Kool, 1995) and the absence of D-loop stacking partners, resulting in the observed accessibility of A_{1106} to DEPC when RNA from in vivo sources was probed (Fig. 4). Consistent with this, differences in accessibilities of the T-loop bases can be detected for modified versus unmodified tRNA (Perret et al., 1990b).

Related TΨC-loops in bromovirus RNA1 and RNA2

As noted in the Introduction, box B sequences matching that in the RNA3 RE are found close to the 5′ ends of BMV RNA1 and 2 (Fig. 1). Like the RNA3 RE, these regions are predicted to fold into an extended hairpin presenting the box B in exact mimicry of a tRNA TΨC-stem loop, and mutational studies in RNA2 support the existence and relevance of this structure for 1a-induced RNA2 stabilization and RNA2 replication (Pogue & Hall, 1992; Chen et al., 2001). Moreover, 5′-proximal box B sequences with the potential to be presented in similar stem loops are conserved in RNA1 and RNA2 of many other viruses in the bromovirus and cucumovirus genuses (Allison et al., 1989; Marsh et al., 1989; Pogue & Hall, 1992; Pogue et al., 1992). In contrast, the box B at the 5′ end of RNA3 conforms to the TΨC-consensus only up to the loop-closing G:C base pair, without being able to actually form a T-stem. This 5′-proximal RNA3 box B sequence most likely becomes part of an alternate, non-tRNA-like hairpin similar to earlier predictions (Pogue & Hall, 1992). This would explain why deletion of the 5′-box B had little or no effect on RNA3 replication in plants (Pogue et al., 1992) and yeast (Sullivan & Ahlquist, 1999), and why the RNA3 5′ noncoding region does not confer 1a-induced stability to heterologous RNAs (Sullivan & Ahlquist, 1999). In keeping with these results, we have found that the 5′ box B sequences in BMV RNA1 and RNA2, but not in RNA3, also are targets for T and Ψ modification in vivo (results not shown). Preliminary results indicate that in vivo modification of box B in RNA1 and RNA2 occurs but is not as efficient as in the RNA3 RE. Further experiments will be required to determine if this is related to the fact that, in BMV infections of natural plant hosts, RNA1 and RNA2 are amplified to lower levels than RNA3 (Kroner et al., 1990).

T and Ψ modifications in the RE box B sequence

Other systems that have evolved tRNA mimicry report modifications similar to the in vivo base modifications of viral RNA reported here. Three uridine positions in the TΨC-stem loop of *E. coli* tmRNA are modified in vivo leading to a conformational stabilization of the

Downloaded from www.rnajournal.org on February 14, 2006

neighboring acceptor stem and a more efficient aminoacylation of the tmRNA at physiological temperatures (Felden et al., 1998). The aminoacylatable 3′ ends of two viral RNAs have been modified in vitro by tRNA nucleotide modifying activities. When incubated in an *E. coli* extract, tobacco mosaic virus RNA was modified at two positions in the TΨC-stem loop of its tRNA-like 3′ end, creating analogs to tRNA T_{54} and 5^mC_{49} (Lesiewicz & Dudock, 1978). Transcripts of the 3′ tRNA-like domain from turnip yellow mosaic virus (TYMV) RNA were modified in vitro by a yeast extract or purified yeast tRNA Ψ synthases at several positions, including T and Ψ modifications in a 7-nt T-loop with only one deviation from the tRNA consensus (Becker et al., 1998). However, attempts to detect modified nucleotides in TYMV RNA extracted from plant cells were not successful (Silberklang et al., 1977). Similarly, as noted in the Results, T or Ψ modifications were not found in the aminoacylatable 3′ end of BMV RNA3 from plant infections or yeast. However, this is less surprising because a suggested T-loop analogy in the BMV 3′ end is far weaker than that in TYMV (Florentz et al., 1982; Rietveld et al., 1983; Felden et al., 1994).

By contrast, the appropriate uridines in the box B/T-loop of the BMV RNA3 RE were efficiently modified to T and Ψ in plant cells and in yeast (Fig. 6). Both in the RNA3 RE (results not shown) and in the corresponding element in RNA2 (Pogue et al., 1990, 1992; Pogue & Hall, 1992; Chen et al., 2001), all mutations interfering with the T-loop mimicry recognized by these modifying enzymes severely inhibit RE function and RNA replication. However, it is not yet clear whether the T and Ψ modifications are required for RE function, or whether they simply reflect strong tRNA T-loop mimicry selected for interaction with other host or viral factors.

MATERIALS AND METHODS

Reagents and enzymes

Aniline was from Fluka; DMS, CMCT, and thiourea were from Aldrich; DEPC, hydrazine, tRNA, and lead acetate were from Sigma; kethoxal was from ICN; yeast RNA was from Boehringer. Restriction enzymes and ribonucleoside vanadyl complex (RVC) were from NEB; T7- and T3-RNA polymerase as well as the Sequitherm EXCEL II cycle-sequencing kit were from Epicentre; lyticase was from Sigma; Superscript II reverse transcriptase was from BRL.

Yeast methods

Yeast strain YPH500 (*MATα ura3-52 lys2-801 ade2-101 trp1-Δ63 his3-Δ200 leu2-Δ1*) was grown to mid-log phase at 30 °C in defined synthetic medium containing 2% galactose as a carbon source (Ausubel et al., 1987). Relevant amino acids were omitted to maintain selection for any plasmid present. Cells were harvested by centrifugation, washed with water, and stored as a pellet corresponding to ~10 OD_{600} per vial at −70 °C. For preparation of spheroplasts, 30–35 OD_{600} of cells were washed successively with water, 1 M sorbitol and SCEMM (1 M sorbitol, 100 mM Na-citrate, pH 5.8, 10 mM EDTA, 30 mM β-mercaptoethanol) and then incubated in 5 mL SCEMM containing 1500 U lyticase for 45 min at 30 °C with occasional gentle swirling. Spheroplasts were harvested by centrifugation at 500 × *g*, washed with SCEMM, and stored at −70 °C in aliquots corresponding to ~5 OD_{600} of starting material.

Plasmids and primers

BMV wild-type RNA3 expression in YPH500 was achieved using the centromeric, TRP1 marker-containing plasmid pB3RQ39 (Ishikawa et al., 1997), in which RNA3 sequence is flanked by the GAL1 promoter and the self-cleaving hepatitis delta ribozyme cassette. BMV 1a was expressed driven by the GAL1 promoter from pB1YT3-H, a centromeric plasmid containing the HIS3 marker (Y. Tomita, M. Ishikawa, & M. Janda, unpubl.). pB3TP8 was used for synthesis of RNA3 without flanking nonviral nucleotides by in vitro transcription with T7 RNA polymerase (Janda et al., 1987) and for production of sequencing ladders. pBS-IGR and pBS-NCR contain the IGR sequence (nt 1004–1222) and the 5′ noncoding region of RNA3 (nt 1–88) cloned between the *Bam*HI and *Eco*O109I sites of a pBluescript SK(−) (Stratagene). pTB18 was derived from pBS-IGR by introducing an internal deletion of the box B (nt 1100–1113) sequence (see Fig. 1, bottom).

Primers T7-OL1 d(AACTGCAGAATTAATACGACTCACTATAGGTAAATCCG) and OL5 d(GCGGTCCAACGATTTCTGCG) were used in PCR on pB3RQ39 to fuse a T7 RNA polymerase promoter to BMV RNA3 cDNA sequence (nt 1004–1324) for in vitro transcription. Similarly, T7-OL1 and T3-Universal (AATTAACCCTCACTAAAGGGA) were used for PCR on pTB18. Primers OL2 d(GCGAGCGCTGATCCAAACGGCTG), OL3 d(ATCCACAAACATGGATAACC TCC), OL4 d(TTTTTTTTTTAATAATAACTCAGACAC) and OL5 were used for primer extension and comparative sequencing reactions.

In vitro transcripts

T7 RNA polymerase run-off transcription using linearized plasmid (pB3TP8, *Eco*RI) or PCR fragments (T7-OL1//OL5, amplified from pB3RQ39, used in full length or cleaved with *Bgl*II immediately after the oligo(A)-coding tract) according to published procedures (Hecker et al., 1988) yielded transcripts of the entire RNA3, IGRcp, and IGR as depicted in Figure 1. PCR template T7-OL1//T3-Universal, amplified from pTB18, was cleaved at the *Spe*I site following the oligo(A)-coding tract and transcribed to obtain $IGR^{\Delta 14}$. (+)- and (−)-strand transcripts for formation of dsIGR and dsNCR were made using plasmids pBS-IGR and pBS-NCR, linearized with either *Kpn*I (−) or *Spe*I (+), in combination with T7- or T3-RNA polymerase. Following transcription, all RNAs were either PAA gel purified (Krupp, 1988) and ethanol precipitated or extracted with phenol/chloroform and chloroform, precipitated twice with ethanol/2.5 M ammonium acetate and purified using AutoSeq G50 spin columns (Pharmacia).

For low salt (LS) structural treatment, transcripts were denatured for 5 min at 95 °C in TE buffer and then snap-cooled

Downloaded from www.rnajournal.org on February 14, 2006

on ice. For high salt (HS) treatment, transcripts were denatured for 5 min at 95 °C in annealing buffer (100 mM NaCl, 50 mM Tris-HCl, pH 8.3, 1 mM EDTA) and then slowly renatured in a styrofoam-covered heat block overnight. Before loading on native gels, samples were dialyzed for 2 h at 4 °C on swim filters (VSWP 25 μm; Millipore) floating on precooled gel electrophoresis buffer.

RNA from in vivo sources

Total RNA from frozen yeast was prepared using mechanical disruption (four rounds of 1 min maximum speed in a Mini-Beadbeater (Biospec Products) followed by 1 min on ice) in combination with the RNeasy mini kit (Qiagen) and stored at −70 °C. Extracts from frozen yeast spheroplasts were prepared on ice by 30× pipetting up and down in 100 μL osmotic lysis buffer containing 50 mM Tris-HCl, pH 7.5, 10 mM RVC, and a mix of protease inhibitors (10 mM benzamidin, 1 mM PMSF, 10 μg/mL aprotinin, 1 μg/mL pepstatin A, and 1 μg/mL leupeptin). For crude fractionation, these extracts were centrifuged for 5 min at 15,000 × *g* and separated into a supernatant and a pellet, which was resuspended in lysis buffer by 20× pipetting, repelleted and, after discarding the second supernatant, again resuspended in 100 μL lysis buffer. Aliquots of total or fractionated extracts were frozen on ethanol/dry ice and stored at −70 °C.

Chemical modification

Buffers and conditions were adapted from Brunel et al. (1991). DMS and DEPC modification in vitro of 0.1 pmol transcripts was performed at room temperature in the presence of 5 μg tRNA in 100 μL of 50 mM Na-cacodylate pH 7.5, 50 mM KCl, 5 mM $MgCl_2$ (native conditions, N) or 100 μL of 50 mM Na-cacodylate pH 7.5, 1 mM EDTA (semidenaturing conditions, SD) and addition of 0.5 μL DMS or 10 μL DEPC, respectively. Modifications in extracts used 12.5 μL total extract (a) or 25 μL supernatant fraction (b) from cells −1a and 25 μL total extract (c) or pellet fraction (d) from cells +1a. Because this corresponded to about 16–12 μg total RNA in (a)–(c), but only 2.5 μg total RNA in (d), the reaction mix was supplemented with 9.5 μg (d) or 12.5 μg (in vitro transcript controls) yeast RNA in the modification reaction. DMS modification in vivo was adapted from Ares and Igel (1990). Two OD_{600} of cells in 500 μL media were incubated with 5 μL DMS for the times indicated and the reaction was stopped by addition of 300 μL ice cold 0.7 M β-mercaptoethanol and 300 μL ice cold isoamyl alcohol. Cells were spun down and washed once with 400 μL 0.7 M β-mercaptoethanol before total RNA was isolated as described above. CMCT modification was performed in vitro as above using 50 mM $Na_2B_4O_7$, pH 8.0, instead of 50 mM Na-cacodylate in the DMS buffers and a final concentration of 4.2 mg/mL (10 mM) CMCT made from a fresh 10× stock in H_2O. Kethoxal modification in vitro used the same conditions and buffers as for DMS with the pH of the 50 mM Na-cacodylate adjusted to 7.0 and a final concentration of 2 mg/mL kethoxal made from a fresh 10× stock in 20% ethanol. Samples treated with kethoxal were exposed to solutions containing 5 mM K-borate at all times thereafter. In vitro modification reactions were stopped after times indicated in the figures by addition of 5 μg tRNA, 350 μL of buffer RLT (RNeasy, Qiagen), and 250 μL ethanol and immediate purification on RNeasy spin columns according to the manufacturer's protocol. Elution with 2× 50 μL H_2O was followed by ethanol precipitation, washing with 70% ethanol and air-drying of the resulting pellets.

RNA chain scission

For the detection of DMS modification at the N7-position of guanosines by primer extension, pellets of modified RNA were dissolved in 10 μL 1 M Tris-HCl, pH 8.3, 10 μL of freshly made 8 mg/mL sodium borohydride were added, and the mixture was incubated for 10 min on ice in the dark (Romby et al., 1987b) followed by ethanol precipitation, washing with 70% ethanol, and air-drying of the resulting pellets. Pellets were taken up in 20 μL of 1 M buffered aniline, pH 4.5 (10 μL aniline + 8 μL glacial acetic acid + 82 μL H_2O), incubated for 10 min at 60 °C, and then lyophilized (Peattie & Gilbert, 1980). Samples were dissolved in 25 μL H_2O and lyophilized two more times. For the detection of DEPC modification at the N7-position of adenines, modified RNA pellets were directly introduced to aniline scission as above without prior borohydride treatment.

Lead cleavage

Cleavage of RNAs with Pb^{2+} was adapted from Krzyzosiak et al. (1988). Twenty-five-microgram extracts prepared (without use of RVC) from 2.5 OD_{600} yeast expressing viral 1a protein and RNA3 or total RNA purified from such extracts were incubated in 50 mM HEPES, pH 7.5, 50 mM KCl, and 5 mM $MgCl_2$, and $Pb(OAc)_2$ was added to final concentrations of 1 mM, 5 mM, and 25 mM and a final volume of 100 μL. Incubation was stopped after 5 min at room temperature by addition of 6 μL 0.5 M EDTA, 350 μL RLT buffer (RNeasy, Qiagen), 250 μL ethanol, and purification over spin columns followed by ethanol precipitation, washing with 70% ethanol, and air-drying of the resulting pellets.

Detection of pseudouridines and ribothymidines

Detection of uridine residues that had been modified in vivo was essentially done as described (Bakin & Ofengand, 1993). In short, 15 μg total RNA extracted from 1.25 OD_{600} yeast cells, 500 ng purified virion RNA (Lane, 1986) + 12.5 μg yeast RNA, or 140 ng RNA3 in vitro transcript (+ yeast RNA) as negative control was lyophilized. For analysis of ribothymidine (5^mU), samples were dissolved in 10 μL fresh mix of hydrazine and H_2O (1:1) and incubated on ice for 2–8 min. Reactions were stopped by addition of 200 μL stop buffer (0.3 M NaOAc, pH 5.7, 0.1 mM EDTA) and 700 μL ethanol and precipitated after 8 min on dry ice. Ethanol pellets were treated with aniline and lyophilized (three times) as above. For analysis of Ψ, RNA was dissolved in 90 μL of Ψ-buffer (50 mM Bicine, pH 8.3, 4 mM EDTA), 10 μL of 43 mg/mL CMCT in Ψ-buffer were added, and incubation was stopped after 20 min at room temperature by addition of 350 μL RLT buffer, 250 μL of ethanol, and purification over RNeasy spin columns (Qiagen) and subsequent ethanol precipitation as

Downloaded from www.rnajournal.org on February 14, 2006

above. For mild alkaline treatment of CMCT-modified RNA, the pellet was dissolved in 40 μL 50 mM Na_2CO_3, pH 10.4, and incubated for 3 h at 37 °C. Reactions were stopped by precipitation with 10 μL 3 M NaOAc, 50 μL H_2O, and 300 μL ethanol and the resulting pellets were air-dried.

Primer extension analysis

Lyophilized RNA from the above treatments was dissolved in 7 μL H_2O, 1 μL of 5′-labeled primers OL2, OL3, OL4, or OL5 (250 fmol, 5×10^5–10^6 cpm) was added, and the RNA denatured for 1 min at 95 °C, then snap-cooled on ice. Two microliters reverse transcriptase (RT) 5× buffer (BRL) was added and annealing proceeded for 20 min at room temperature. To this, 2 μL RT 5× buffer, 2 μL 0.1 M DTT, 2 μL 10 M dNTP, 2 μL H_2O, 0.5 μL RNasin® and 0.5 μL (100 U) Superscript II RT were added. After 90 min at 48 °C, the RT reaction was stopped and the template degraded by addition of 5 μL 3 M KOH, incubation at 95 °C for 3 min, addition of 25 μL 50 mM Tris-HCl, pH 8.0, 7.5 mM EDTA, 0.5% SDS, and further incubation at 40 °C for 2 h (Brunel et al., 1991). RT products were precipitated with 6 μL 3 M acetic acid, 6 μL 3 M NaOAc, and 200 μL ethanol, dissolved in 12 μL formamide loading solution, and 6 μL were applied per lane on 6% or 8% PAA (19:1) denaturing gels containing 8 M urea and 0.5× TBE. Sequencing reactions were prepared by cycle-sequencing 5 μg plasmid pB3TP8 with 0.5 pmol ($1–2 \times 10^6$ cpm) of the same labeled primer used in the RT reaction.

Computer-based structure predictions

Calculation of the RNA3 secondary structures was carried out using Michael Zuker's web-based *mfold 3.0* (Mathews et al., 1999; Zuker et al., 1999) fixed to 37 °C and set to 5% suboptimality and no limit on the maximum base pair distance. Prediction of conserved secondary structure was done using the program package ConStruct (Lück et al.,1999) on a Macintosh G4 in a Linux 2000PPC environment. In this, IGR sequences from BMV (GenBank accession number V00099), CMV subgroup I (strain/GenBank number FT/1339927, Pepo/1339930, Mf/7242509, CS/1339933, Y/U61160, N/1339924, C7-2/575931, E5/575932, NGP/U61159, Fny/222018, M/222021, Kor/L36251, 86-212/U61161), CMV subgroup II (Kin/Z12818, Passiflora/U61162, Wemmershoek/U61163, Lupin K5/U61164, Trk7/L15336), TAV (C/D01015, 1/7530172, V/7530168, B/S72468, P/L15335), and PSV (J/D00668, W/U31366, ER/NC_002040) were aligned by PileUp (Genetics Computer Group, 2001), and individual partition functions at 37 °C and resulting dot plots were generated to yield a common consensus dot plot and consensus structure. Each sequence in a closely related subgroup of *n* was given a weight of 1/*n* to account for the different numbers of sequences available for each subgroup. Gaps in the alignment were optimized manually for maximum structure formation.

ACKNOWLEDGMENTS

We thank Dr. Petra Klaff and Dr. Jean-Marc Lanchy for valuable recommendations regarding chemical mapping; Dr. Michael Schmitz and Dr. Gerhard Steger for long-distance help with establishing and running the ConStruct program; and Dr. Michael L. Sullivan for sharing clones, unpublished results, and helpful advice. This research was supported by the National Institutes of Health through Grant GM35072. P.A. is an investigator of the Howard Hughes Medical Institute.

Received June 28, 2001; returned for revision August 8, 2001; revised manuscript received August 21, 2001

REFERENCES

Ahlquist P. 1992. Bromovirus RNA replication and transcription. *Curr Opin Gen Dev 2*:71–76.

Ahlquist P, Dasgupta R, Kaesberg P. 1981. Near identity of 3′ RNA secondary structure in bromoviruses and cucumber mosaic virus. *Cell 23*:183–189.

Ahola T, Ahlquist P. 1999. Putative RNA capping activities encoded by brome mosaic virus: Methylation and covalent binding of guanylate by replicase protein 1a. *J Virol 73*:10061–10069.

Allison R, Thompson C, Ahlquist P. 1990. Regeneration of a functional RNA virus genome by recombination between deletion mutants and requirement for cowpea chlorotic mottle virus 3a and coat genes for systemic infection. *Proc Natl Acad Sci USA 87*: 1820–1824.

Allison RF, Janda M, Ahlquist P. 1989. Sequence of cowpea chlorotic mottle virus RNAs 2 and 3 and evidence of a recombination event during bromovirus evolution. *Virology 172*:321–330.

Ares M Jr, Igel AH. 1990. Lethal and temperature-sensitive mutations and their suppressors identify an essential structural element in U2 small nuclear RNA. *Genes & Dev 4*:2132–2145.

Ausubel FM, Brent R, Kingston RE, Moore DD, Seidman JG, Smith JA, Struhl K, eds. 1987. *Current protocols in molecular biology*. New York: John Wiley & Sons.

Bakin A, Ofengand J. 1993. Four newly located pseudouridylate residues in *Escherichia coli* 23 S ribosomal RNA are all at the peptidyltransferase center: Analysis by the application of a new sequencing technique. *Biochemistry 32*:9754–9762.

Bastin M, Hall TC. 1976. Interaction of elongation factor 1a with aminoacylated brome mosaic virus RNA. *J Virol 20*:117–122.

Baumstark T, Riesner D. 1996. Only one of four possible secondary structures of the central conserved region of potato spindle tuber viroid is a substrate for processing in a potato nuclear extract. *Nucleic Acids Res 23*:4246–4254.

Becker HF, Motorin Y, Florentz C, Giegé R, Grosjean H. 1998. Pseudouridine and ribothymidine formation in the tRNA-like domain of turnip yellow mosaic virus RNA. *Nucleic Acids Res 26*:3991–3997.

Becker HF, Motorin Y, Sissler M, Florentz C, Grosjean H. 1997. Major identity determinants for enzymatic formation of ribothymidine and pseudouridine in the TΨ-loop of yeast tRNAs. *J Mol Biol 274*:505–518.

Björk GR. 1992. The role of modified nucleosides in tRNA interactions. In: Hatfield D, Lee BJ, Pirtle RM, eds. *Transfer RNA in protein synthesis*. Boca Raton, Florida: CRC Press. pp 23–85.

Boccard F, Baulcombe D. 1993. Mutational analysis of *cis*-acting sequences and gene function in RNA3 of cucumber mosaic virus. *Virology 193*:563–578.

Brown RS, Hingerty BE, Dewan JC, Klug A. 1983. Pb(II)-catalyzed cleavage of the sugar-phosphate backbone of yeast $tRNA^{Phe}$—implications for lead toxicity and self-splicing RNA. *Nature 303*: 543–546.

Brunel C, Romby P, Westhof E, Ehresmann C, Ehresmann B. 1991. Three-dimensional model of *Escherichia coli* ribosomal 5 S RNA as deduced from structure probing in solution and computer modeling. *J Mol Biol 221*:293–308.

Butcher SE, Dieckmann T, Feigon J. 1997. Solution structure of a GAAA tetraloop receptor RNA. *EMBO J 16*:7490–7499.

Chapman M, Kao CC. 1999. A minimal RNA promoter for minus-strand RNA synthesis by the brome mosaic virus polymerase complex. *J Mol Biol 286*:709–720.

Chen J, Ahlquist P. 2000. Brome mosaic virus polymerase-like pro-

Downloaded from www.rnajournal.org on February 14, 2006

tein 2a is directed to the endoplasmic reticulum by helicase-like viral protein 1a. *J Virol 74*:4310–4318.
Chen J, Noueiry A, Ahlquist P. 2001. Brome mosaic virus protein 1a recruits viral RNA2 to RNA replication through a 5′ proximal RNA2 signal. *J Virol 75*:3207–3219.
Davanloo P, Sprinzl M, Watanabe K, Albani M, Kersten H. 1979. Role of ribothymidine in the thermal stability of transfer RNA as monitored by proton magnetic resonance. *Nucleic Acids Res 6*:1571–1581.
Davies C, Symons RH. 1988. Further implications for the evolutionary relationships between tripartite plant viruses based on cucumber mosaic virus RNA3. *Virology 165*:216–224.
Davis DR. 1995. Stabilization of RNA stacking by pseudouridine. *Nucleic Acids Res 23*:5020–5026.
Dirheimer G, Keith G, Dumas P, Westhof E. 1995. Primary, secondary and tertiary structures of tRNAs. In: Söll D, RajBhandary UL, eds. *tRNA: Structure, biosynthesis, and function.* Washington, DC: ASM Press. pp 93–140.
Draper DE. 1999. Themes in RNA–protein recognition. *J Mol Biol 293*:255–270.
Dreher TW, Bujarski JJ, Hall TC. 1984. Mutant viral RNAs synthesized in vitro show altered aminoacylation and replicase template activities. *Nature 311*:171–175.
Ehresmann C, Baudin F, Mougel M, Romby P, Ebel JP, Ehresmann B. 1987. Probing the structure of RNAs in solution. *Nucleic Acids Res 15*:9109–9128.
Farkas WR. 1968. Depolymerization of ribonucleic acids by plumbous ions. *Biochim Biophys Acta 155*:401–409.
Felden B, Florentz C, Giegé R, Westhof E. 1994. Solution structure of the 3′-end of brome mosaic virus genomic RNAs: Conformational mimicry with canonical tRNAs. *J Mol Biol 235*:508–531.
Felden B, Hanawa K, Atkins JF, Himeno H, Muto A, Gesteland RF, McCloskey JA, Crain PF. 1998. Presence and location of modified nucleotides in *Escherichia coli* tmRNA: Structural mimicry with tRNA acceptor branches. *EMBO J 17*:3188–3196.
Florentz C, Briand JP, Romby P, Hirth L, Ebel JP, Giegé R. 1982. The tRNA-like structure of turnip yellow mosaic virus RNA: Structural organization of the last 159 nucleotides from the 3′-OH terminus. *EMBO J 1*:269–276.
French R, Ahlquist P. 1987. Intercistronic as well as terminal sequences are required for efficient amplification of brome mosaic virus RNA3. *J Virol 61*:1457–1465.
French R, Janda M, Ahlquist P. 1986. Bacterial gene inserted in an engineered RNA virus: Efficient expression in monocotyledonous plant cells. *Science 231*:1294–1297.
Genetics Computer Group. 2001. *Wisconsin Package Version 10.0.* Madison, Wisconsin.
Gorbalenya AE, Koonin EV. 1993. Helicases: Amino acid sequence comparisons and structure-function relationships. *Curr Opin Cell Biol 3*:419–429.
Grosjean H, Edqvist J, Stråby KB, Giegé R. 1996. Enzymatic formation of modified nucleosides in tRNA: Dependence on tRNA architecture. *J Mol Biol 255*:67–85.
Grosjean H, Houssier C, Romby P, Marquet R. 1998. Modulatory role of modified nucleotides in RNA loop-loop interaction. In: Grosjean H, Benne R, eds. *Modification and editing of RNA.* Washington, DC: ASM Press. pp 113–133.
Gu X, Santi DV. 1991. The T-arm of tRNA is a substrate for tRNA (m^5U54)-methyltransferase. *Biochemistry 30*:2999–3002.
Gu X, Yu M, Ivanevitch KM, Santi DV. 1998. Molecular recognition of tRNA by tRNA pseudouridine 55 synthase. *Biochemistry 37*:339–343.
Haseloff JP, Goelet D, Zimmern P, Ahlquist P, Dasgupta R, Kaesberg P. 1984. Striking similarities in amino acid sequence among nonstructural proteins encoded by RNA viruses that have dissimilar genomic organization. *Proc Natl Acad Sci USA 81*:4358–4362.
Hecker R, Wang Z, Steger G, Riesner D. 1988. Analysis of RNA structures by temperature gradient gel electrophoresis: Viroid replication and processing. *Gene 72*:59–74.
Hermann T, Patel DJ. 2000. RNA bulges as architectural and recognition motifs. *Structure 8*:R47–R54.
Inoue T, Cech TR. 1985. Secondary structure of the circular form of the *Tetrahymena* rRNA intervening sequence: A technique for RNA structure analysis using chemical probes and reverse transcriptase. *Proc Natl Acad Sci USA 82*:648–652.
Ishikawa M, Janda M, Krol MA, Ahlquist P. 1997. In vivo DNA expression of functional brome mosaic virus RNA replicons in *Saccharomyces cerevisiae. J Virol 71*:7781–7790.
Janda M, Ahlquist P. 1993. RNA-dependent replication, transcription and persistence of brome mosaic virus RNA replicons in *S. cerevisiae. Cell 72*:961–970.
Janda M, Ahlquist P. 1998. Brome mosaic virus RNA replication protein 1a dramatically increases in vivo stability but not translation of viral genomic RNA3. *Proc Natl Acad Sci USA 95*:2227–2232.
Janda M, French R, Ahlquist P. 1987. High efficiency T7 polymerase synthesis of infectious RNA from cloned brome mosaic virus cDNA and effects of 5′-extensions on transcript infectivity. *Virology 158*:259–262.
Joshi RL, Joshi S, Chapeville F, Haenni HL. 1983. tRNA-like structures of plant viral RNAs: Conformational requirements for adenylation and aminoacylation. *EMBO J 2*:1123–1127.
Karasawa A, Nakaho K, Kakutani T, Minobe Y, Ehara Y. 1991. Nucleotide sequence of RNA3 of peanut stunt cucumovirus. *Virology 185*:464–467.
Kong F, Sivakumaran K, Kao CC. 1999. The N-terminal half of the brome mosaic virus 1a protein has RNA capping-associated activities: Specificity for GTP and S-adenosylmethionine. *Virology 259*:200–210.
Koshlap KM, Guenther R, Sochacka E, Malkiewicz A, Agris PF. 1999. A distinctive RNA fold: The solution structure of an analogue of the yeast $tRNA^{Phe}$ TΨC domain. *Biochemistry 38*:8647–8656.
Kroner PA, Young BM, Ahlquist P. 1990. Analysis of the role of brome mosaic virus 1a protein domains in RNA replication, using linker insertion mutagenesis. *J Virol 64*:6110–6120.
Krupp G. 1988. RNA synthesis: Strategies for the use of bacteriophage RNA polymerases. *Gene 72*:75–89.
Krzyzosiak WJ, Marciniec T, Wiewiorowski M, Romby P, Ebel JP, Giegé R. 1988. Characterization of the lead(II)-induced cleavages in tRNAs in solution and effect of the Y-base removal in yeast $tRNA^{Phe}$. *Biochemistry 27*:5771–5777.
Lane LC. 1986. Propagation and purification of RNA plant viruses. *Methods Enzymol 118*:687–696.
Lankat-Buttgereit B, Gross HJ, Krupp G. 1987. Detection of modified nucleosides by rapid RNA sequencing methods. *Nucleic Acids Res 15*:7649.
Lesiewicz J, Dudock B. 1978. In vitro methylation of tobacco mosaic virus RNA with ribothymidine-forming tRNA methyltransferase. Characterization and specificity of the reaction. *Biochim Biophys Acta 520*:411–418.
Loesch-Fries LS, Hall TC. 1982. In vivo aminoacylation of brome mosaic and barley stripe mosaic virus RNAs. *Nature 298*:771–773.
Louise-May S, Auffinger P, Westhof E. 1996. RNA structure from molecular dynamics simulation. In: Sarma RH, Sarma MH, eds. *Biological structure and dynamics*, Vol 2. Schenectady, New York: Adenine Press. pp 73–91.
Lück R, Gräf S, Steger G. 1999. ConStruct: A tool for thermodynamic controlled prediction of conserved secondary structure. *Nucleic Acids Res 27*:4208–4217.
Marsh LE, Pogue GP, Hall TC. 1989. Similarities among plant virus (+) and (−) RNA termini imply a common ancestry with promoters of eukaryotic tRNAs. *Virology 172*:415–427.
Mathews DH, Sabina J, Zuker M, Turner DH. 1999. Expanded sequence dependence of thermodynamic parameters improves prediction of RNA secondary structure. *J Mol Biol 288*:911–940.
Miller WA, Hall TC. 1983. Use of micrococcal nuclease in the purification of highly template dependent RNA-dependent RNA polymerase from brome mosaic virus-infected barley. *Virology 125*:236–241.
Misra VK, Draper DE. 1999. On the role of magnesium ions in RNA stability. *Biopolymers 48*:113–135.
Nagaswamy U, Voss N, Zhang Z, Fox GE. 2000. Database of noncanonical base pairs found in known RNA structures. *Nucleic Acids Res 28*:375–376.
O'Reilly D, Thomas CJ, Coutts RH. 1991. Tomato aspermy virus has an evolutionary relationship with other tripartite RNA plant viruses. *J Gen Virol 72*:1–7.
Pacha RF, Ahlquist P. 1991. Use of bromovirus RNA3 hybrids to study template specificity in viral RNA amplification. *J Virol 65*:3693–3703.

Downloaded from www.rnajournal.org on February 14, 2006

Peattie DA, Gilbert W. 1980. Chemical probes for higher-order structure in RNA. *Proc Natl Acad Sci USA 77*:4679–4682.

Perret V, Garcia A, Grosjean H, Ebel JP, Florentz C, Giegé R. 1990a. Relaxation of a transfer RNA specificity by removal of modified nucleotides. *Nature 334*:787–789.

Perret V, Garcia A, Puglisi J, Grosjean H, Ebel JP, Florentz C, Giegé R. 1990b. Conformation in solution of yeast $tRNA^{Asp}$ transcripts deprived of modified nucleotides. *Biochimie 72*:735–744.

Pogue GP, Hall TC. 1992. The requirement for a 5′ stem-loop structure in brome mosaic virus replication supports a new model for viral positive-strand RNA initiation. *J Virol 66*:674–684.

Pogue GP, Marsh LE, Hall TC. 1990. Point mutations in the ICR2 motif of brome mosaic virus RNAs debilitate (+)-strand replication. *Virology 178*:152–160.

Pogue GP, Marsh LE, Connell JP, Hall TC. 1992. Requirements for ICR-like sequences in the replication of brome mosaic virus genomic RNA. *Virology 188*:742–753.

Quadt R, Ishikawa M, Janda M, Ahlquist P. 1995. Formation of brome mosaic virus RNA-dependent RNA polymerase in yeast requires coexpression of viral proteins and viral RNA. *Proc Natl Acad Sci USA 92*:4892–4896.

Quadt R, Kao CC, Browning KS, Hershberger RP, Ahlquist P. 1993. Characterization of a host protein associated with brome mosaic virus RNA-dependent RNA polymerase. *Proc Natl Acad Sci USA 90*:1498–1502.

Restrepo-Hartwig M, Ahlquist P. 1996. Brome mosaic virus helicase and polymerase-like proteins colocalize on the endoplasmic reticulum at sites of viral RNA synthesis. *J Virol 70*:8908–8916.

Restrepo-Hartwig M, Ahlquist P. 1999. Brome mosaic virus RNA replication proteins 1a and 2a colocalize and 1a independently localizes on the yeast endoplasmic reticulum. *J Virol 73*:10303–10309.

Rietveld K, Pleij CWA, Bosch L. 1983. Three-dimensional models of the tRNA-like 3′-termini of some plant viral RNAs. *EMBO J 2*: 1079–1085.

Romby P, Carbon P, Westhof E, Ehresmann C, Ebel JP, Ehresmann B, Giegé R. 1987a. Importance of conserved residues for the conformation of the T-loop in tRNAs. *J Biomol Struct Dyn 5*: 669–687.

Romby P, Moras D, Dumas P, Ebel JP, Giegé R. 1987b. Comparison of the tertiary structure of yeast $tRNA^{Asp}$ and $tRNA^{Phe}$ in solution. *J Mol Biol 195*:193–204.

Saenger W. 1984. Principles of nucleic acid structure. In: Cantor CR series ed. *Springer Advanced Texts in Chemistry*. New York: Springer Verlag.

Schmitz U, Donati A, James TL, Ulyanov NB, Yao L. 1998. Small structural ensembles for a 17-nucleotide mimic of the tRNA TΨC-loop via fitting dipolar relaxation rates with the quadratic programming algorithm. *Biopolymers 46*:329–342.

Sengupta R, Vainauskas S, Yarian C, Sochacka E, Malkiewicz A, Guenther RH, Koshlap KM, Agris PF. 2000. Modified constructs of the tRNA TΨC domain to probe substrate conformational requirements of m^1A58 and m^5U54 tRNA methyltransferase. *Nucleic Acids Res 28*:1374–1380.

Silberklang M, Prochiantz A, Haenni AL, Rajbhandary UL. 1977. Studies on the sequence of the 3′-terminal region of turnip-yellow-mosaic-virus RNA. *Eur J Biochem 72*:465–478.

Simorre JP, Legault P, Hangar AB, Michiels P, Pardi A. 1997. A conformational change in the catalytic core of the hammerhead ribozyme upon cleavage of an RNA substrate. *Biochemistry 36*: 518–525.

Sivakumaran K, Kao CC. 1999. Initiation of genomic positive-strand synthesis from DNA and RNA templates by a viral RNA-dependent RNA polymerase. *J Virol 73*:6415–6423.

Smirnyagina E, Hsu YH, Chua N, Ahlquist P. 1994. Second-site mutations in the brome mosaic virus RNA3 intercistronic region partially suppress a defect in coat protein mRNA transcription. *Virology 198*:427–436.

Sprinzl M, Horn C, Brown M, Ioudovitch A, Steinberg S. 1998. Compilation of tRNA sequences and sequences of tRNA genes. *Nucleic Acids Res 26*:148–153.

Steger G, Baumstark T, Mörchen M, Tabler M, Tsagris M, Sänger HL, Riesner D. 1992. Structural requirements for viroid processing by RNase T1. *J Mol Biol 227*:719–737.

Sullivan ML, Ahlquist P. 1997. *Cis*-acting signals in bromovirus RNA replication and gene expression: Networking with viral proteins and host factors. *Semin Virol 8*:221–230.

Sullivan ML, Ahlquist P. 1999. A brome mosaic virus intergenic RNA3 replication signal functions with viral replication protein 1a to dramatically stabilize RNA in vivo. *J Virol 73*:2622–2632.

Tinoco I Jr, Bustamante C. 1999. How RNA folds. *J Mol Biol 293*: 271–281.

Traynor P, Ahlquist P. 1990. Use of bromovirus RNA2 hybrids to map *cis*- and *trans*-acting functions in a conserved RNA replication gene. *J Virol 64*:69–77.

Van Regenmortel MHV, Fauquet CM, Bishop DHL, Carstens E, Estes M, Lemon S, Maniloff J, Mayo MA, McGeoch D, Pringle CR, Wickner RB, eds. 2000. *Virus taxonomy. Seventh report of the International Committee on Taxonomy of Viruses.* New York/San Diego: Academic Press.

Wang S, Kool ET. 1995. Origins of the large difference in stability of DNA and RNA helices: C5-methyl and 2′-hydroxyl effects. *Biochemistry 34*:4125–4132.

Wang YX, Huang S, Draper DE. 1996. Structure of a U:U pair within a conserved ribosomal RNA hairpin. *Nucleic Acids Res 24*: 2666–2672.

Westhof E, Dumas P, Moras D. 1983. Loop stereochemistry and dynamics in transfer RNA. *J Biomol Struct Dyn 1*:337–355.

Westhof E, Dumas P, Moras D. 1985. Crystallographic refinement of yeast aspartic acid transfer RNA. *J Mol Biol 184*:119–145.

Yao LJ, James TL, Kealey JT, Santi DV, Schmitz U. 1997. The dynamic NMR structure of the TΨC-loop: Implications for the specificity of tRNA methylation. *J Biomol NMR 9*:229–244.

Zuker M, Mathews DH, Turner DH. 1999. Algorithms and thermodynamics for RNA secondary structure prediction: A practical guide. In: Barciszewski J, Clark BFC, eds. *RNA Biochemistry and Biotechnology.* NATO ASI Series. Dordrecht, The Netherlands: Kluwer Academic Publishers. pp 11–43.